Electromagnetic technology for prospecting unconventional hydrocarbon resources

Liangjun Yan[1,2,3]

[1]Key Laboratory of Exploration Technologies for Oil and Gas Resources (Yangtze University), Ministry of Education, China, 430100. yljemlab@163.com
[2]Cooperative innovation center of Unconventional oil and gas, Hubei, China
[3]Key Laboratory of Geophysical prospecting, CNPC

SUMMARY

Unconventional oil and gas (normally tight gas and oil, shale gas and oil, coal seam gas, natural gas hydrate, etc.), which generally have the characteristics of source-reservoir symbiosis, are widely distributed. Still, their high-quality reservoirs have large burial depths, small targets, complex electrical properties, and considerable inhomogeneity, making their a great challenge for electromagnetic (EM) exploration to detect them. In recent decade, A series of achievements have been made in the field of EM exploration of unconventional oil and gas worldwide, including the EM response mechanism of unconventional reservoir rocks, new methods and technologies in controlled-source EM exploration on land, identification and evaluation methods for oil and gas using EM parameters. These technologies have been successfully applied in unconventional oil and gas exploration and development with good effect and have been recognized by petroleum geology and development circles. Firstly, this paper introduced the complex resistivity characteristics of organic-rich shale, tight sandstone, and dolomite in southern China occurring in low porosity and permeability reservoirs, and discovered that organic-rich shale has the characteristics of low resistivity and high polarization. At next, an IP model for the shale reservoirs is established. Based on the mechanism of source-reservoir symbiosis in shale reservoirs, the identification mode for the sweet spot is proposed. It is then proved this paper that there exist a good petrophysics foundation for the EM exploration in the field of shale gas exploration and development. Secondly, there has been a research focus on how to use the multiple IP parameters, such as resistivity and polarizability, to estimate the characteristic parameters of the sweet spot of reservoir. The prediction method based on IP model for the parameters of reservoir is introduced. Thirdly, there is an outspring of the controlled-source EM exploration methods for unconventional oil and gas exploration, such as Wide Field Electromagnetic Method (WFEM), Wire-less Electromagnetic Method (WEM), Time-Frequency Electromagnetic Method (TFEM), Long Offset and Window Transient Electromagnetic Method (LowTEM) and Focused Source Electromagnetic Method (FSEM). These methods and technologies share a common feature of using a long wire source, with high-power, large current multi-waveform transmission, multi-component array acquisition and hybrid processing and inversion. Therefore, not only the signal-to-noise ratio, exploration depth, resolution and reliability, but also the efficiency, resolution, cost and adaptability have been significantly improved, making these methods able to deal with the geology problems in the exploration and development of unconventional oil and gas under complex conditions. Finally, several cases are given to indicate the apparent application effects of the new methods and technologies of controlled-source EM method in unconventional oil and gas exploration, sweet spot detection, fluid identification, fracturing monitoring, and at the same time, look into the broad application prospect of EM methods in the exploration and development of unconventional oil and gas. However, there are still plenty of unsuccessful cases. It is a long way to go in the effective application of EM methods in unconventional oil and gas exploration and development. Therefore, more achievements are expected to be made, especially on the EM response mechanism of unconventional oil and gas reservoirs, 3D high spatial and temporal density data collection technology under complex geological and topographical conditions, fast, stable and reliable high-precision inversion and imaging methods with constraints based on prior logging and seismic data, reservoir parameters prediction method based on refined IP model.
Due to the limitation of the author's ability and the paper's length, the new methods, technologies, and application cases referred to in this paper are mainly from China.

INTRODUCTION

Due to the greenhouse effect and environmental concerns, human's yearn for clean energy has been inspired. However, the conventional oil and gas resources shortage has been a global headache in

the Post-Petroleum Era, therefore, the exploitation and development of unconventional oil and gas reserves are gaining more and more attentions worldwide among governments and energy companies. Unconventional oil and gas resources including tight gas and oil, shale gas and oil, heavy oil, coal seam gas, and natural gas hydrate, are significant parts of the global energy structure, which occupy about 80% of the total oil and gas reserves on the earth. The successful development of unconventional oil and gas resources, especially shale gas and tight sandstone gas in the United States (US) has enabled the country to become self-sufficient in natural gas for the first time in the last over 40 years. In 2009, the output of unconventional natural gas in the US first exceeded that of conventional natural gas. Since then, the US turned into an important shale gas exporter and the supply pattern of the global natural gas market has changed. China is the world's second-largest energy consumer, and its unconventional oil and gas reserves is equivalent to the US. To meet the social needs and to reduce the energy dependency, China has accelerated the research on unconventional oil and gas related geological theories, exploration technologies, development methods and technical equipment. So far, many advances have been made and huge achievements have been achieved. With the continuous rising of unconventional oil and gas output, the national energy structure is considerably improved.

1.1 Geological and geophysical characteristics of unconventional oil and gas reservoirs

● Geological characteristics

Unconventional oil and gas resources are different kinds of oil/gas reserves that cannot be explored and developed simply with regular technologies and methods. Generally, the reservoir forming conditions of unconventional oil and gas resources are less demanding than those of conventional oil and gas resources, thus, unconventional reservoirs are more common and their occurrence modes are more diverse, Unconventional reservoirs possess the following geological characteristics (Zou, 2015):
(a) source-reservoir symbiosis;
(b) large distribution area, deep burial depth, and blurred boundaries;
(c) tight, poor physical properties, low porosity, low permeability, extensive nanoscale cracks, and strong heterogeneity;
(d) lithological diversity (sandstone, limestone, shale, coal and migmatite, etc.), small effective reservoir;
(e) rich in organic matter, high maturity, poor phase segregation, no unified boundaries of oil, gas, and water.
● Geophysical characteristics
Reservoir rocks containing oil and gas usually

possess the characteristics of high resistivity and high polarization (Zonge,1975; Lima and Sharma, 1992; Sigel et al., 2007; Davydycheva et al., 2006; Burtman, 2015; Hu 2022). He and Wang (2007) proposed the 'Ring three storey' model for oil and gas identification based on EM and IP parameters. They confirmed that oil-gas reservoirs were of high resistivity and high polarization, while the water-bearing reservoirs were generally of low resistivity and high polarization. Based on the spatial resistivity and polarization differences, oil, gas and water could be easily and effectively identified. With this model, numerous favorable geological results have been obtained by applying the EM method in oil and gas exploration (He, 2005; Davydycheva, 2006; He, 2010). However, the differences in geological characteristics make the electrical features of unconventional reservoirs noticeably different. Unconventional reservoirs are mainly shale, mud shale, tight sandstone, and mudstone, which present the features of low resistance, low permeability and low polarization. A great quantity of petrophysical experiments indicated that shale gas reservoirs in southern China generally demonstrated the characteristics of low density, low speed, high resistance, and low magnetism (Wang, 2015). By conducting substantive complex resistivity measurements, Yan et al. (2014) and Xiang et al. (2014) found that rich-organic shale in southern China had the characteristics of low resistivity and high polarization. Similar results were obtained by Burtman (2014) using TerraTek shale rock samples. Similarly, changes in electrical characteristics are also noticeable during thermal flooding and hydraulic fracturing process. For example, when SAGD technique is applied, steam chambers and possible steam channeling-paths may form, and phase-transformation zones would form surround the steam-injection wells. The resistivity variations within different phase-transformation zones can provide physical-property foundation to identify the steam-flooding front. (Yang et al. 2005; Hu, 2022). As for hydraulic fracturing in shale gas reservoir, low resistance and high polarization anomalous body would form when thousands of tons of fracturing fluid are injected into the reservoir (Chen, 2000). Therefore, EM method can be used to monitor the spatial distribution of fracturing fluid and shed light on fracturing optimization.

1.2 Exploration features of unconventional oil and gas

Unconventional reservoirs demonstrate different source, lithology and physical properties, as well as hydrocarbon conditions from conventional reservoirs, thus, the exploration methods, development and evaluation techniques can be totally different. To explore the unconventional oil

and gas reservoirs, there are three stages: firstly, screen out the core area based on the high-quality reservoir evaluation criteria; secondly, identify the 'Sweet Spots Area (Segment)' based on the reservoir integral/local tectonic characteristics, and fault and microfracture features; finally, drilling, production and 'Sweet Spots Area (Segment)' evaluation. Compared with conventional oil and gas, there are three changes in unconventional reservoirs exploration (Zou, 2015), one is from 'finding oil in trap' to 'finding oil in the strata', second is from 'oil/gas reservoir' to 'oil/gas layer', and third is from 'Sweet Spot' to 'Sweet Spot Area (Segment)'. The 'Sweet Spot Area (Segment)' of unconventional reservoirs refers to as the source-reservoir symbiosis development area, which is an unconventional hydrocarbon enrichment area with large distribution range, specific thickness, high-quality source rock, good physical properties, high oil/gas saturation, high formation energy (i.e., high gas-oil ratio, high formation pressure), high brittleness index, rich fracture and local structure developed. Evaluation and optimization of "Sweet Spots Area (Segment)" is the key of unconventional oil and gas exploration and development, which runs through the whole exploration and development process. The evaluation parameters slightly vary with different unconventional reservoirs. The main evaluation parameters include TOC, porosity, the development degree of microfractures, brittleness, range (burial depth and distribution area), etc. (Zou et al., 2015; Yang, 2019). To improve the economic recovery efficiency of unconventional reservoir, it is necessary to improve reservoir permeability or fluid viscosity by horizontal drilling, fracturing, and other techniques to guarantee the continuous or quasi continuous accumulation of oil/gas resources. According to the specific geological problems and electrical characteristics in the three stages of unconventional oil and gas exploration, EM exploration technology can give full play to the advantages to achieve the exploration, detection and evaluation of sweet spots.

1.3 Opportunities and challenges of EM exploration technologies

Due to the limitation of inherent method and theory, EM exploration is far less important than seismic exploration in oil and gas exploration, and only applied in the early stage of oil and gas exploration in basin survey. In unconventional reservoirs, the difference of seismic wave impedance between oil, gas and water is small, which makes seismic exploration difficult (Yuan, 2013). However, the difference of resistivity and dielectric constant between oil, gas and water is very large, and electromagnetic method has superior conditions for fluid identification and sweet spot detection (Yan,

2014). The high-power EM method can capture the high-resolution anomaly field distribution caused by resistivity and polarizability differences. When combined with seismic exploration methods, the distribution of 'Sweet Spots Area (Segment)', residual oil distribution, spatial distribution of steam or water injected can be elaborately described, and the reservoir permeability and oil/gas saturation can be accurately predicted. With the development of unconventional and ultra-deep oil and gas exploration, the cost of seismic exploration is increasing and the exploration is becoming more and more difficult. Electromagnetic exploration methods are facing great opportunities as well as severe challenges.

● Inherent limitations of EM methods

The essential difference between EM and seismic methods lies indifferent field properties. Seismic wave field belongs to the wave field, while electromagnetic field belongs to the diffusion field. Low-frequency EM methods are generally used for oil and gas exploration, which can be easily affected by volume effect, static offset, field source effect, overprint effect, shadow effect, etc. Fortunately, the development of high-precision 3D EM modeling technique has provided an effective tool to mitigate these adverse effects. For instance, the joint inversion of multiple field sources can effectively suppress the field source effect (He, 2019). Fictitious wave transformation for transient electromagnetic field improves the interpretation reliability and resolution (Chen, 1999; Li, 2005; Mittet, 2015, 2018; Stoffa et al. 2018). Full domain, full coverage, full waveform field, and uniform illumination three-dimensional EM data acquisition and processing, special wave field transformation and inversion imaging techniques are the keys to overcome the limitations of the EM exploration methods.

● EM response mechanism of reservoir rocks

EM response mechanism is closely related to the reservoir physical properties. The simplified resistivity model based EM methods is now facing great challenges to solve complicate geological problems, and the induced polarization (IP) mechanism of reservoir rocks should be valued (Kavian, 2012; Fiandaca, 2012). The time and frequency dispersion characteristics caused by the fluids and minerals in reservoir should be comprehensively considered and studied (Burtman, 2014, 2015). Meanwhile, the physical and structural characteristics of the conventional and unconventional oil and gas reservoirs should be distinguished, and an equivalent complex resistivity model comprehensively considering EM induction, IP and other effects should be established (Zhdanov, 2008). Moreover, the foundation of controllable source electromagnetic (CSEM) technology should be established based on the IP mechanism of reservoir rocks. Only by fully utilizing the sensitivity

of the IP parameters in complex resistivity model can the purpose of precise multi-parameter joint detection of oil and gas be realized. Therefore, it is essential to study the IP mechanism and anomaly extraction method of unconventional oil and gas reservoirs to improve the detection accuracy and the interpretation reliability. It is an inevitable trend in the development of EM exploration to seek IP multi-parameters based CSEM method.

● EM data acquisition

The effectiveness of exploration highly relies on the space-time density and the quality of EM data, and data acquisition technique is the prerequisite and the guarantee for the development of EM exploration methods. Acquisition technology requires a deep combination of methods, instruments, acquisition software, field geology and terrain conditions, geological targets and other factors, through feasibility analysis and simulation test, to develop an effective acquisition scheme. Firstly, In the acquisition method, it is necessary to achieve a substantial breakthrough in 3D acquisition, realize multi-field source coverage and uniform illumination, and synchronize acquisition with hundreds of thousands of instruments to record massive electromagnetic multi-component time series data, so as to meet the requirements of high spatial and temporal density data for high precision inversion. Secondly, high-quality acquisition software capable to conduct noise level analysis, feasibility analysis and data quality evaluation should be developed to improve the exploration efficiency. Finally, portable, intelligent, low-cost, low-power and low-noise EM multichannel receivers should also be manufactured to simplify the acquisition process.

● EM data processing

Data processing is significant part of the successful application of EM methods. Without a proper data processing technique, no matter how sensitive the instrument, how advanced the data collection techniques, and how high the quality of data, the results obtained will be worthless. Data processing mainly include data preprocessing, attribute parameter definition and extraction. Denoising and correcting is the first step in the data processing. Due to the cultural noise and the signal distortion caused by the method or the geological and topographical factors, targeted de-noising and correction methods are required. Many modern signal processing methods have been adapted to data de-noising, such as the robust estimation, median filtering, wavelet transform, recursive flood wave, and coherent analysis methods (Kass & Li 2011; Streich, 2011; Ji et al. 2016; Rasmussen et al. 2017; Wu, 2021). In contrast, the correction methods, such as the field source correction and static shift correction, are developed based on the characteristics of the methods. Because of the complexity of EM methods and noise, there is no

universal correction and denoising techniques. Attribute parameter extraction is guaranteed to improve the reliability and effect of the inversion and interpretation. Conventional method is to define the apparent resistivity parameter. However, the complicated multidimensional source creates great difficulties in defining the apparent resistivity. Thus, using different field components or combinations of methods to define the attribute parameters by numerical calculations, such as the all-time apparent resistivity and all-time vertical conductivity, oil-water identification factor, differentially normalized quantities, has attracted research interest, and several good application results have been achieved (Yan, 1999; Davydycheva et al., 2006; He, 2015; Xue, 2020; He, 2021).

● EM inversion and interpretation methods

Theoretically, all geophysical inversions are underdetermined problems. It is difficult to infer the information about the abnormal underground targets accurately from a single type of geophysical data. Comprehensive inversion and interpretation by multiple geophysical datasets are becoming a significant research trend. Joint inversion using as many types of prior information as possible is an effective means of reducing the multiplicity of inversion, improving the data utilization, and modifying the inconsistency of the inversion model. Seismic information is relatively abundant in oil and gas exploration, and the method of joint inversion of EM and seismic data has attracted research attention and achieved better specific results (Peng and Liu, 2020, He, 2020). In unconventional oil and gas exploration, EM signals are sensitive to the sweet spot, and the electrical properties are consistent with the characteristic parameters, such as the porosity, brittleness, permeability, and TOC. With the constraints provided by the reservoir information obtained from the seismic data, the inversion resolution and interpretation reliability can be improved using EM data to predict the reservoir parameters. Furthermore, this method can reduce the risk of exploration and development.

There are two types of joint inversion: one type is based on petrophysical relationships and the other is based on structural similarity relationships (Peng and Liu, 2020). In oil and gas exploration and development, petrophysical and geological information can be acquired as the prior information. Integrating the prior information, such as petrophysical and geological data, into the inversion can reduce the non-uniqueness of the optimization problems and help obtain proper inversion results (Giraud et al., 2017; Astic and Oldenburg, 2019). Joint inversion based on the empirical relationships among the various geophysical parameters has undergone vigorous development (Jegen et al., 2009; Heincke et al., 2010; Lelievre et al., 2012), and the petrophysical empirical or statistical formula can be applied in industry. Via the intersection

analysis of the P-wave velocity and resistivity, Jegen et al. (2009) obtained the sectional empirical relationship between the P-wave velocity and resistivity. They confirmed that the empirical relationship can be locally effective under a specific geological background. Xu et al. (2016) and Peng et al. (2018) created marine EM and seismic data joint inversion frameworks based on the relationship between the reservoir and petrophysics and using the Archie formula and Gassmann formula, respectively. They both achieved global optimization one-dimensional joint inversion and extracted the reservoir porosity and saturation information. Hu et al. (2020) utilized the prior information obtained from the logging and seismic profile to perform constraint modeling, and they realized the artificial fish swarm joint inversion using the magnetotelluric (MT) and gravity data. Yang et al. (2021) proposed the petrophysical relationship between the velocity and resistivity based on the cross-variation function, and then, they adopted the guided fuzzy c-means clustering algorithm to carry out the multi-constraint inversion and completed the two-dimensional MT and seismic data joint inversion. However, there is still no standard petrophysical model that can link all of the physical parameters. Therefore, it is difficult to the directly integrate the petrophysical or other geological features into a standard geophysical inversion (Astic and Oldenburg, 2019).

Compared with the constrained inversion based on the empirical petrophysical relationship, the joint inversion built via structural coupling requires less prior information. Haber and Oldenburg (1997) first proposed the concept of structural coupling constraint inversion, and Gallando and Meju (2003 and 2004) subsequently proposed the cross-gradient inversion method. Multiple parameters joint inversion based on spatial structure similarity has gradually become the mainstream algorithm. Hu et al. (2009) applied the cross-gradient algorithm technique to joint inversion of two-dimensional seismic and EM data with multiplicative regularization and showed that the reservoir evaluation based on the joint inversion was better than that obtained through imaging interpretation of the individual seismic data. Zhdanov (2012) proposed a universal spatial structure constraint algorithm named Gramian spatial constraint method. It has many choices of operators for Gramian space; and when the operator is transformed into a gradient type, the cross-gradient method is obtained. Lelievre and Farquharson (2013) obtained a linear variation expression of the local model parameters and a solution for the change rate in all directions using the construction method, constructed Gramian spatial constraint operator using the obtained gradient of the model parameters, and finally achieved joint inversion of multiple datasets. Gao et al. (2017) proposed a cross-gradient joint inversion strategy using alternately updating model parameters, which reduced the complexity of algorithm. Yan et al. (2020) derived the three-dimensional (3D) discrete form of the cross-gradient operator and realized 3D joint inversion of gravity, magnetic, and MT data. Currently, the joint inversion of seismic and EM data is based on the petrophysical information constraints. Research on the structural coupling algorithm has primarily focused on joint inversion of gravity, magnetic, and EM data, and structural coupling joint inversion using seismic and EM data is the future goal in unconventional oil and gas EM exploration.

1.4 Level and ability of the EM exploration method

The EM method is an effective means of resource and energy exploration. The physical property foundation is the differences of the resistivity, dielectric constant, and polarization in rocks. The detection of underground geological targets can be realized by observing the spatial-temporal distribution of the EM fields. Although EM method has a good electrical basis in unconventional oil and gas exploration, the sweet spots of unconventional oil and gas reservoirs feature large burial depth, small target and strong heterogeneity, which require higher resolution, exploration depth and level of data processing and interpretation of electromagnetic exploration method. In the last 20 years of development, the methods of petroleum EM exploration have been comprehensively improved. In terms of the instruments, geophysical instrument companies such as Phoenix, Zong, KMS, Metronix, and Geonics have developed various types of high-power and strong current transmitting systems and multi-functional networked portable receivers. The wide frequency electromagnetic instrument developed by China's Jishan High-tech company, the high-power time-frequency electromagnetic system developed by BGP, CNPC, and the ultra-high power and ultra-low frequency transmitting and receiver developed by the Institute of Geophysics, Chinese Academy of Sciences, have also been put into oil and gas exploration. The Mag-power transmitter through a few kilometers to dozens of kilometers long ground wire to feed hundreds of amperes of current underground, can be convenient to emit a variety of waveform, for the time domain and frequency domain electromagnetic method to provide a powerful source of electromagnetic field. Low power consumption, broadband, low noise level, large dynamic range, portable, light weight, multi-function, distributed receivers can realize the data acquisition to thousands of channels array, which provided a hardware guarantee for 3D EM data acquisition and hydraulic fracturing monitoring under complex geology and terrain conditions. Lots of new control

source EM methods were emerging to improve the resolution, detection depth, and interpretation reliability, such as the Wide Frequency EM method (WFEM), Wire-less EM method (WEM), Time-frequency EM method (TFEM), Long offset, long window Transient EM method (LowTEM), and Focused Source EM method (FSEM). These methods have greatly improved the anti-noise ability, detection depth, resolution, reliability, work efficiency, cost, and adaptability. The use of new data processing, 3D inversion and interpretation techniques had significantly enhanced the ability of electromagnetic methods to serve unconventional oil and gas exploration. At the same time, the study of unconventional reservoir rocks physics of has been deepening, and the induced polarization mechanism of unconventional reservoirs has made new progress. The model that accurately describes the IP mechanism of unconventional reservoirs has been preliminarily established, and the parameter prediction method of unconventional reservoirs based on this model has also been basically formed (Tong, 2020; Burtman, 2015).

Lots of reviewers have summarized the EM methods and technologies in oil and gas exploration and development (He, 2010,2019; Strack, 2013,2014;Tietze 2014; Streich 2015; Di 2019, 2020; Xue 2016, 2020; Constable, 2010; Liu 2021). This paper focuses on the study of electrical characteristics of unconventional reservoir, the sweet spot detection and its characteristic parameters prediction methods based on the IP model, as well as the research progresses in regarding the new methods and technologies in EM exploration. In addition, several cases studies of shale gas the sweet spot detection and hydraulic fracturing monitoring with LowTEM were presented. The summary of the cases studies will benefit the wide application of new EM methods and technologies in unconventional oil and gas exploration and development.

2. Sweet spot detection and its character parameters prediction

The detection and evaluation technology of shale gas sweet spot is the key to shale gas exploration and development. Seismic exploration method undoubtedly plays an important role in sweet spot detection and development because of their high resolution and attribute identification capability. However, most of the shale gas exploration areas in southern China are rugged areas, and covered by limestone, seismic exploration is much more expensive and difficult to obtain high-quality data. In addition, the sweet spots are distributed in argillaceous source rocks with deep burial depth, high degree of evolution and rich organic matter. The seismic impedance characteristics are not obvious and there are no clear trap characteristics.

The shale reservoir itself is a source rock with extremely low porosity and permeability, and strong heterogeneity. As a result, the seismic characteristics of the sweet spot are not obvious, which makes prediction difficult. Therefore, the development of high-precision seismic prediction methods for shale gas reservoirs faces great challenges, and the development of cost-effective non-seismic methods is an effective way to detect sweet spot in unconventional reservoirs.

As the most effective supplementary means of seismic exploration, the electromagnetic (EM) exploration method has the advantages of large exploration depth, high work efficiency, low cost and strong adaptability, and has been playing an important role in the early stage of basin oil and gas exploration. The EM exploration of oil and gas based on EM diffusion can only be effective when the resistivity of the oil and gas reservoir is high enough compared with the surrounding rocks. The importance of IP effect in rocks has been realized, and two IP parameters (resistivity and chargeability) have been tried to jointly detect oil and gas reservoirs (Davydycheva, 2006; He, 2010; Commer, 2011). Complex resistivity (CR) method, which is based on the IP theory, has been tried to identify conventional oil and gas in China for more than 30 years (Wu, 1996; Xu,2004; Su et al., 2005), and two kinds of IP anomaly models were put forward to interpret the CR date. One considered that the reservoir itself was a dynamic multiphase balance system, in which the double electric layer formed from bi-phase medium, and was the source in which the IP field came from (He, 2007). Another was called 'the micro-seepage model' which considered IP effect happened above the reservoir because the hydrocarbons migrated to the upper reducing zone, and resulted in the formation of the rich pyrite halo which was the source of strong IP effect (Veeken, 2009).

Shale gas is stored in the reservoir in free or adsorbed state, and has the typical characteristics of self-generation and self-storage and in-situ accumulation, which inevitably determines the difference in the IP anomaly model of data interpretation in shale gas exploration. Are the above two models suitable for shale gas exploration? What are the geoelectric characteristics of organic-rich shale? Does the shale gas reservoir have a strong IP effect? Can the resistivity and chargeability be integrated to identify the sweet spot? What is the sweet spot detecting pattern for EM exploration? Yan et al., (2014), Xiang (2014) collected hundreds of shale samples in southern China, performed compositional analysis, complex resistivity and Total Organic Carbon (TOC) measurements, and found a qualitative relationship between pyrite content and TOC. On this basis, combined with the IP theory study, the methods to predict the sweet spot's characteristic parameters

and the detection pattern suitable for EM method were proposed.

2.1 Electrical characteristics of shale in southern China

Xiang et al. (2014) collected 243 geological outcrop samples in Yibin, Sichuan and Zunyi, Guizhou in southern China. The lithologies are mainly organic-rich shale, sandstone, dolomite and basalt (surrounding rock formations). Through the complex resistivity measurement and analysis, the IP parameters of the samples were obtained, and the physical properties of each formation were shown in Figure 1 and Table 1. Compared with the surrounding sandstone, dolomite and basalt, the average resistivity of the organic-rich shale is about 120 $\Omega \cdot m$, and the average polarizability is about 20% in Wufeng Group-Longmaxi Group; the average resistivity of the organic-rich shale is about 147 $\Omega \cdot m$, and the average polarizability is about 42% in the Qiongzhusi Group. These indicated that the organic-rich shale exhibited the characteristics of low resistivity and high chargeability, which was inconsistent with the low chargeability characteristics of conventional shale reservoirs.
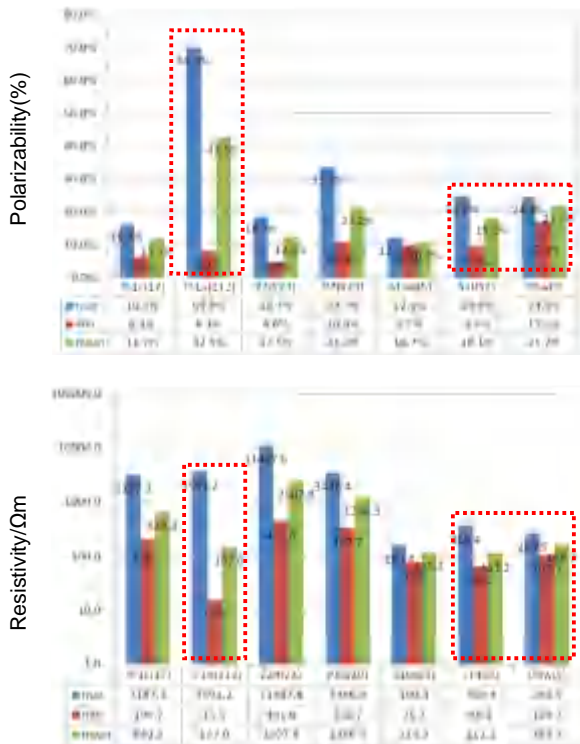
Figure 1. Polarizability and resistivity results of CR measurement for geological outcrop rocks at different groups (top: chargeability; bottom: resistivity)

2.2 Prediction of the sweet spot characteristic parameters

● TOC predicting

Organic-rich shale is abundant in Zhaotong, Yunnan, with shallow burial depth and large thickness. China National Petroleum Corporation (CNPC) has made breakthroughs in shale gas exploration in this area. The Well Z104 has successfully produced industrial gas, with a daily gas production of 20,000 cubic meters. The logging curves of Well Z104 (Figure 2) showed that the shale gas reservoir had obvious characteristics of low resistivity, low velocity and high gamma value. The mineral composition analysis of 34 cores from the groups of S_1l-O_3w and $\text{\textepsilon}_1n$ in Well Z104 showed that the average content of quartz and feldspar was 30% to 60%, the average content of carbonate minerals is generally less than 30% (except mud shale), the average content of clay minerals is 10% to 35%, the content of pyrite is generally high, with a maximum value of 20% and an average content of 5% (Figure 3).
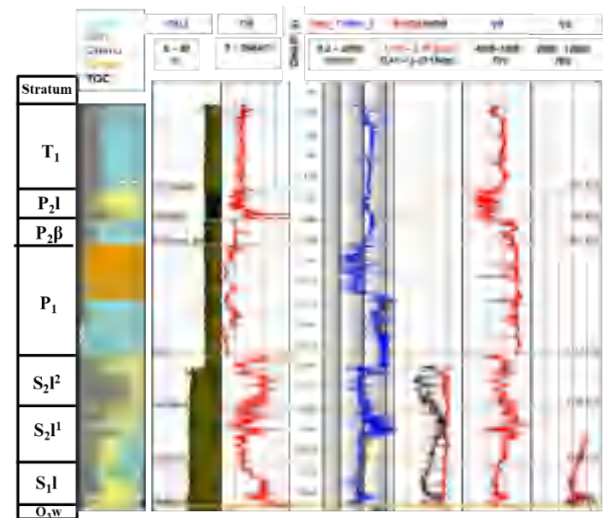

**Figure 2.** Z104 Geology Histogram and Logging Curves
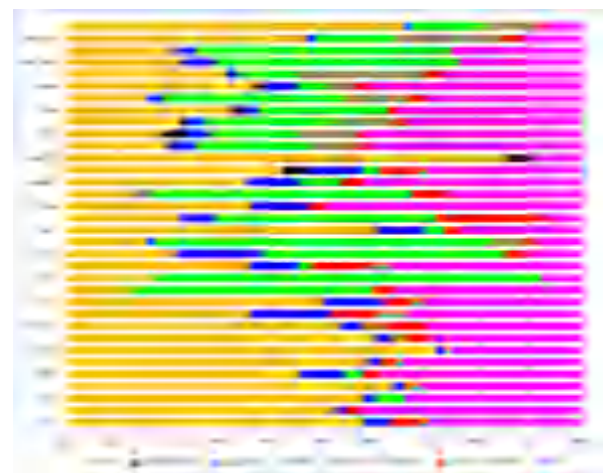
Figure 3. The mineral composition in the shales from S_1 l-O_3w and $\text{\textepsilon}_1$n (red: pyrite)

The complex resistivity measurement and TOC analysis were performed on 11 cores from Well Z104. Figure 4 indicated that the chargeability was

consistent with the variation of pyrite content, with a high positive correlation. Figure 5 presented a plot of TOC and pyrite content versus chargeability. The results showed that there was also a good correspondence between pyrite content and TOC. Apparently, pyrite is an indicator mineral for IP, and is it also an indicator mineral for TOC? If the relationship between TOC and chargeability could be established, it will have great significance for EM exploration.

Why is pyrite abundant in organic-rich shales? Is it necessarily related to TOC? A significant phenomenon is that pyrite is not only a characteristic mineral formed in organic-rich deposits, but also a marker of sedimentary environment and a characteristic mineral of strong IP effect. Veeken (2009) explained its formation process and controlling factors. The depositional environment of shale was a deep-water anoxic environment (reduction reaction environment), coupled with its self-generation and self-storage reservoir characteristics, the increase in TOC acted as a catalyst, providing a chemical reaction environment for the formation of secondary pyrite in the shale clay, the chemical process was as follows

$$CH_4 + Ca^{2+} + SO_4^{2-} \rightarrow CaCO_3 + H_2S \uparrow + H_2O$$

$$H_2S + Fe^{2+} + 2OH^- \rightarrow FeS_2 + H_2O$$
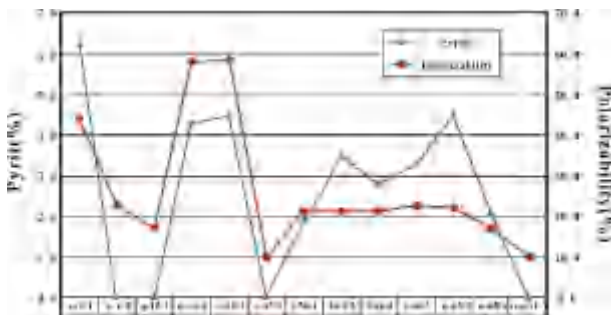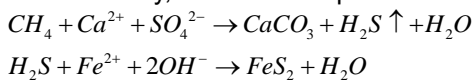
Figure 4. Relationship between pyrite and polarizability
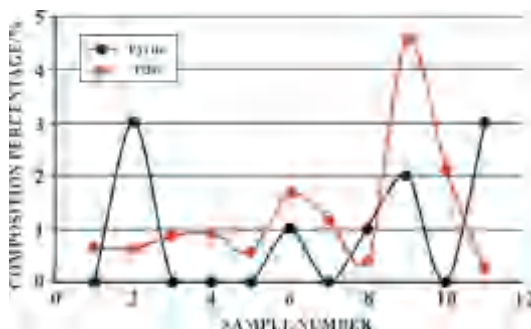
Figure 5. Relationship between TOC and pyrite

In addition, biodegradation and bacterial activity might give rise to organic origin of pyrite in the sedimentary pile. It was proved empirically that significant enrichment in pyrite was often related to hydrocarbon occurrences at deeper levels.

Based on the resistivity, polarizability and TOC of

organic-rich shale, Xiang (2016) and Xu (2020) gave an empirical relationship model between polarizability and TOC, as shown in Figure 6.


$$y = -13.048x^2 + 21.038x - 1.2677$$
$$R^2 = 0.888$$
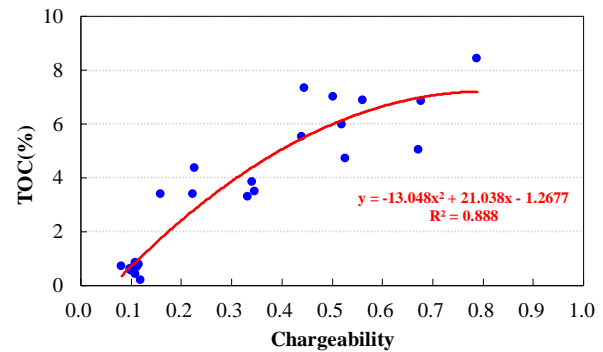
Figure 6. The Cross-plot of TOC and Polarizability

● Prediction of brittleness index

The mineral composition of shale reflected the depositional environment and depositional conditions of shale, and also determines the brittleness index of shale, which affects the fracturing and development of shale gas. It is of great significance to study the relationship between brittleness index and electrical parameters from the perspective of shale mineral composition. Quartz content is the main reason for the shale's brittleness, but the roles of other important brittle minerals cannot be ignored. There were many definitions of brittleness index. Xu et al. (2020) defined the brittleness index B as follows:

$$B = \frac{quartz + feldspar + Pyrite}{quartz + feldspar + Pyrite + carbonate + clay} \quad (1)$$

The above formula highlighted the relationship between pyrite content, brittleness index and electrical parameters (resistivity and polarizability). The brittleness of Well Z104 shale was statistically analyzed by formula (1), and the relationship between the brittleness index and the polarizability was established, as shown in Figure 7. It can be seen that the quadratic nonlinear relationship was obvious


$$B = 18.772\ln(m) + 81.373$$
$$R^2 = 0.9229$$
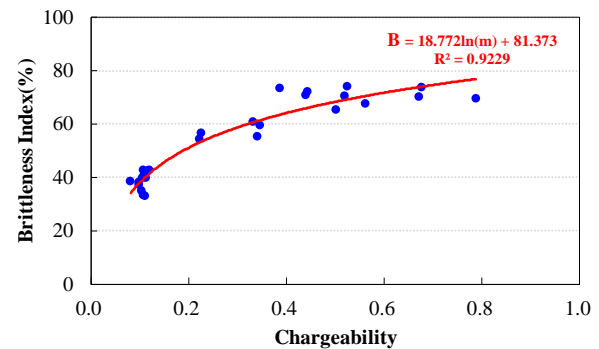
Figure 7. The cross-plot of brittleness index and polarizability

● Prediction of the permeability

Unconventional reservoirs usually have low porosity

and low permeability characteristics (porosity less than 10%, pore throat diameter less than 1 μm or permeability less than 1 mD). In order to achieve sustainable and effective oil and gas production, it is necessary to combine horizontal well drilling, formation fracturing and other technologies to increase reservoir permeability or reduce fluid viscosity (Zou et al., 2013).
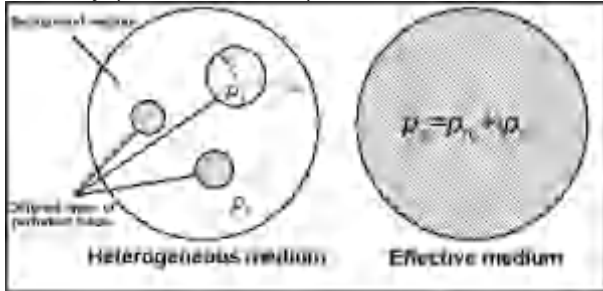

Figure 8. The schematic diagram of the effective-medium theory. A heterogeneous media contains many different types of perturbed media, each of which contains resistivity ρ_l , effective radius r_l , and surface-polarizability coefficient α_s^l . The resistivity of heterogeneous medium is equivalent to the CR of an effective medium through the effective-medium approach. (Tong et al., 2020)

Combining theoretical and experimental analysis of the electromagnetic characteristics of the 'sweet spot' region, establishing the theoretical relationship model between electromagnetic response and reservoir physical properties is the key to realize the EM detection and quantitative evaluation of sweet spot. Reservoir physical properties such as porosity, saturation, and permeability are sensitive parameters for reservoir IP characteristics (Slater, 2007). Archie (1942) gave the empirical relationship between pure sandstone conductivity and formation water conductivity, connected porosity and formation water saturation. However, the rock mineral composition and pore structure of unconventional reservoirs with low porosity and low permeability was complex, and the Archie's relationship was no longer applicable. The polarization effects (electric double layer polarization, Maxwell-Wagner dielectric polarization, etc.) existing at the interface of different minerals and pore fluids will cause the IP phenomenon of reservoir in the electromagnetic exploration frequency range. Pelton et al., (1978) first used the Cole-Cole model to characterize rock IP phenomena, and it was widely used in EM exploration. Zhdanov (2008) proposed the generalized effective-medium theory of induced polarization (GEMTIP) model based on strict mathematical and physical equations. GEMTIP is suitable for IP problems in anisotropic and multiphase media, and established a quantitative relationship between model parameters and rock physical properties, which is more conducive to

reservoir prediction. Tong et al., (2020) extended the theoretical relationship between macroscopic IP parameters and microstructure in the GEMTIP, and established MGEMTIP model under the assumption of isotropic spherical perturbation (Figure 8). MGEMTIP：

$$\rho_e = \frac{\rho_0}{M_0}\left\{1+\sum_{l=1}^{N}\eta_l\left[1-\frac{1}{i\omega\tau_l+1}\right]\right\}^{-1} \qquad (2)$$

where $M_0 = 1-\sum_{l=1}^{N}3f_l/2$, $\eta_l = 9\rho_0 f_l/\left[M_0(4\rho_l+2\rho_0)\right]$,

$\tau_l = r_l/\left[2\alpha_s^l(2\rho_l+\rho_0)\right]$. ρ_0 is the DC resistivity of the background medium, $f_l, \rho_l, r_l, \alpha_s^l$ respectively correspond to the volume component of the l type perturbed medium, DC resistivity, equivalent spherical radius and surface polarization parameters N is the total amount of perturbed medium, the equivalent medium polarizability is

$\eta_t = \sum_{l=1}^{N}\eta_l$. The relationship between η_t and the polarizability m of the Cole-Cole model is $m = \eta_t/(1+\eta_t)$. MGEMTIP is consistent with the polarization characteristics of discrete metallic minerals (Wong, 1979), and also explains the high polarization phenomenon in which the Mawell-Wagner polarization shifts to low frequencies under high oil saturation condition (Burtman and Zhdanov, 2015).

The electrical Kozeny-Carman (K-C) equation characterized the rock porosity and tortuosity through the formation factor F , and characterized the capillary radius r through the specific surface area S_{por} . The permeability relationship can be expressed as

$$k = \frac{Q}{F^b S_{por}^c} \qquad (3)$$

Where Q, b, c are the fitting parameters (Slater, 2007).Since the seepage in unconventional reservoirs was dominated by the diffusion of non-Darcy flow, the validity of the electrical K-C equation was greatly reduced in low permeability rocks. Many studies proposed to use complex resistivity to estimate, thereby improving the prediction accuracy of permeability (Börner et al. 1996; de Lima and Niwas 2000; Slater and Lesmes 2002). Figure 9 showed the permeability prediction relationship based on normalized polarizability (Weller et al., 2015), but there was a large error in the prediction results of low permeability rocks. Figure 10 showed that S_{por} correlated with the imaginary conductivity σ'' (which mainly controls the polarizability strength), but the quantitative relationship needed to be further determined in combination with clay minerals (Revil et al., 2013). Conductive minerals

such as clay and metals in unconventional reservoirs usually do not participate in the seepage process, but directly affect the rock IP phenomenon.
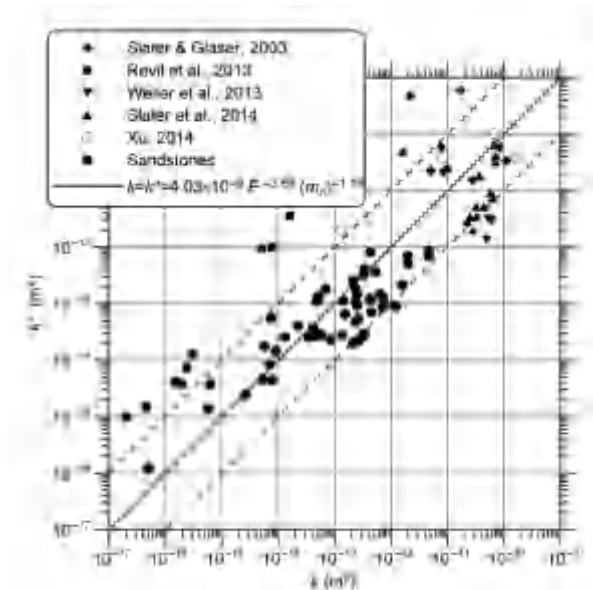

Figure 9. Permeability relationship between experimental measurement and electrical K-C model estimation based on normalized polarizability m_n ($m_n = m\sigma_0$)(Weller et al., 2015)
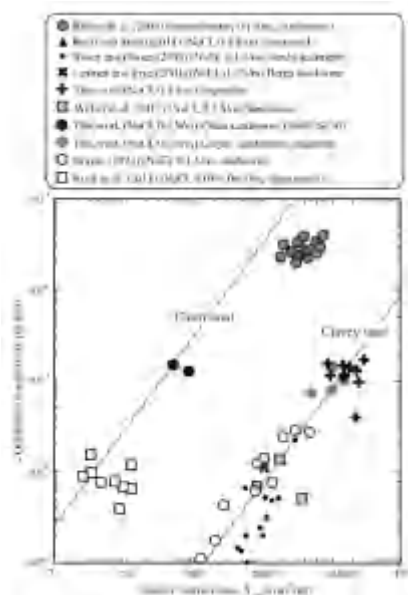

Figure 10. Experimental relationship between the imaginary conductivity and specific surface area between sandstone and clayey sandstone (Revil et al., 2013)

Whether conductive minerals actually produce conductance or polarization can be effectively analyzed by combining the mineral size, connectivity, and frequency band (Vinegar and Waxman, 1984; Xiang et al., 2014; Revil et al., 2015). Numerical simulations showed that there was a nonlinear effect between the permeability of
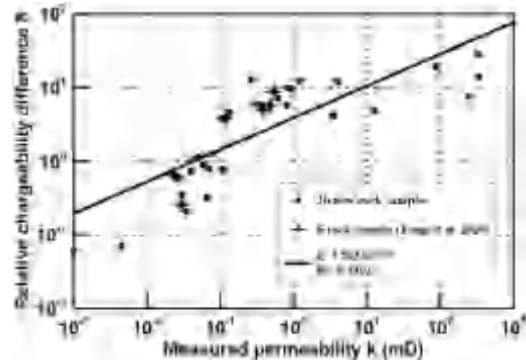
Figure 11. Relationship between relative polarizability difference and permeability of tight rock
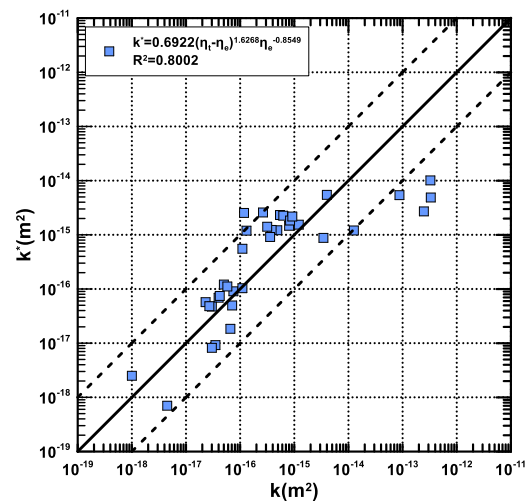
Figure 12. Permeability relationship between experimental measurement and MGEMTIP estimation based on polarizability difference

fractured tight reservoirs (limestone) and the conductivity of formation water (Kirkby et al., 2016). The electrical characteristics of these unconventional reservoirs seriously affect the permeability prediction based on the electrical K-C model. The existence of clay and minerals in unconventional reservoirs makes it difficult to distinguish the IP mechanism of unconventional reservoirs. Removing or suppressing polarization independent of pore fluid can effectively improve the prediction accuracy of permeability. There is a difference between the theoretical polarizability of the MGEMTIP (no seepage) and the measured polarizability of tight rocks (weak seepage). This difference has a good correlation with the rock permeability (Figure 11). The permeability prediction formula based on MGEMTIP was proposed

$$k^* = \frac{Q(\eta_t - \eta_e)^b}{\eta_e^c} = \frac{Q\Delta\eta^b}{\eta_e^c} \qquad (4)$$

Where η_t and η_e correspond to the theoretical polarizability and measured polarizability of the rock, and Q, b, c are the rock characteristic indices. With

this model a good permeability prediction for low-porosity and low-permeability rocks containing low-resistivity minerals was achieved (Figure12).

2.3 Geo-electrical mode for sweet spot detection

Based on the complex resistivity test and analysis of unconventional reservoir rocks, there were three understandings: first, the excitation polarization of sweet spot was mainly generated by electron-conducting minerals such as pyrite, and its IP mechanism is the electron polarization mechanism. Second, the sweet spot region is characterized by high polarization and low resistivity. Third, the sweet spot area, its IP anomaly and resistivity anomaly overlap in space. Based on these three understandings, the geo-electrical mode of electromagnetic exploration for sweet spot was put forth(Yan, 2014；Figure 13). This mode provided a theoretical basis for the EM detection and comprehensive interpretation of sweet spot.
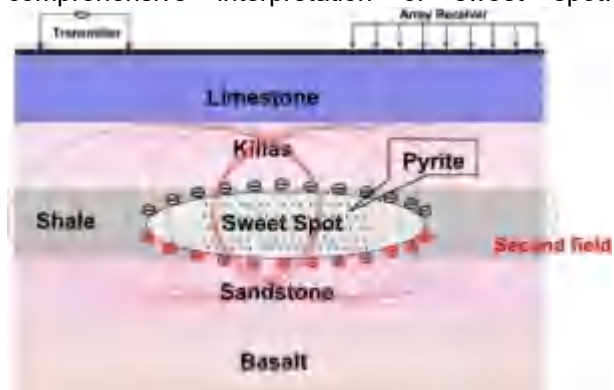
Figure 13. Sketch map of geo-electrical mode for sweet spot detection

3. The innovations in CSEM on land

In recent years, based on the development of methods and instruments, especially that of the CSAMT (Goldsten, 1975), CR (Zonge, 1975), LOTEM (Strack, 1989), and MTEM(Hobbs, 2006), a variety of new CSEM methods with a significant improvement in the adaptability, anti-interference ability, exploration depth, inversion effect, and resolution ability have been developed. These methods, including the TFEM, WEM, and FCEM, LowTEM are currently being applied in unconventional oil and gas exploration and development, and they possess the following innovations.

3.1 Definitions of EM property parameter

● Models and field components of the EM property parameter definitions

Because the horizontal electrical dipole has better attenuation characteristics in terms of offset and frequency than the magnetic dipole, the grounded line CSEM method has been generally applied in oil and gas and deep structure exploration. The horizontal electric field, the vertical magnetic field/the induced electromotive force (EMF) are the typical observed components. In terms of interpretation parameter definition, in addition to the uniformly conductive and non-polarized half-space model, the uniformly conductive and polarized half-space model and the earth-ionosphere model have also been developed, as shown in figure 14.
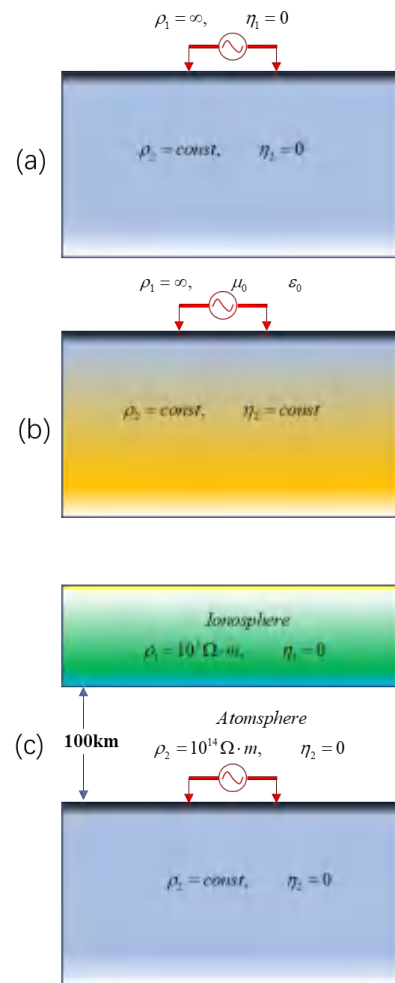

Figure 14. (a) conductive non-polarized half-space model; (b) conductive polarized half-space model and (c) the earth-ionosphere model

For the uniformly conductive and non-polarized half-space model, the time-domain electric and magnetic fields of the electric dipole were expressed as follows(Piao, 1990):

$$E_x = \frac{Idl\rho}{2\pi r^3}[\Phi(u) - \sqrt{\frac{2}{\pi}}ue^{-u^2/2}] \tag{5}$$

$$\frac{\partial H_z}{\partial t} = \frac{Idl\sin\theta}{\pi\mu_0 r^4}[\Phi(u) - \sqrt{\frac{2}{\pi}}u(1+\frac{u^2}{3})e^{-u^2/2}] \tag{6}$$

the frequency-domain electric and magnetic fields of the electric dipole were expressed as follows:

$$E_x = \frac{Idl\rho}{2\pi r^3}[3\cos^2\varphi - 2 + (1+ikr)e^{-kr}] \tag{7}$$

$$H_z = -\frac{3Idl\sin\theta}{2\pi k^2 r^4}[1 - e^{ikr}(1 + ikr - \frac{1}{3}k^2 r^2)] \tag{8}$$

where $k = \sqrt{-i\omega\mu/\rho}$.

For the uniformly conductive and polarized half-space model, the time-domain electric field of the electric dipole can be written as follows (Davydycheva, 2006):

$$
\begin{aligned}
E_x(t) = \frac{Idl\rho}{2\pi r^3}\Bigg\{ & \left[\mathrm{erf}(u) - \frac{2u}{\sqrt{\pi}}e^{-u^2}\right] \\
& + \eta e^{n^2/u^2}\left[1 - \mathrm{erf}(\frac{n}{u})\right] \\
& + \eta\left[\mathrm{erf}(u) - \frac{2nu}{\sqrt{\pi}}\right]e^{-u^2} \\
& + \eta e^{n^2/u^2}e^{2n}\left[1 - \mathrm{erf}(\frac{n}{u} + u)\right] \\
& \times(1 - 2n + 2n^2)\Bigg\}
\end{aligned}
\tag{9}
$$

Where $u = \sqrt{\frac{\mu_0}{2\rho t}}r$, r is the offset, t is the observation time, ρ is the resistivity of the homogeneous half space, $n = 0.5r\sqrt{\sigma\mu/\tau}$.

For the earth-ionosphere model, the expressions of the EM components of the ground source were as follows (Li, 2015):

$$
\begin{aligned}
E_x = & i\omega\mu\frac{Idl}{4\pi}\int_0^\infty F\cdot\mathrm{J}_0(\lambda r)\mathrm{d}\lambda \\
& + \frac{i\omega\mu}{k_1^2}\frac{Idl}{4\pi}\cos^2\theta\int_0^\infty(FF - \frac{k_1^2}{\lambda^2}F)\cdot\lambda^2\cdot\mathrm{J}_0(\lambda r)\mathrm{d}\lambda \\
& + \frac{i\omega\mu}{k_1^2}\frac{P_E}{4\pi}\frac{1}{r}(1 - 2\cos^2\theta)\int_0^\infty(FF - \frac{k_1^2}{\lambda^2}F)\cdot\lambda\cdot\mathrm{J}_1(\lambda r)\mathrm{d}\lambda
\end{aligned}
\tag{10}
$$

$$
\begin{aligned}
H_y = & \frac{Idl}{4\pi}\int_0^\infty -\frac{u_1}{R_1(0)}F\cdot\mathrm{J}_0(\lambda r)\mathrm{d}\lambda \\
& + \frac{Idl}{4\pi}\frac{1}{r}(1 - 2\cos^2\theta)\int_0^\infty\left[-\frac{R_1^*(0)}{u_1}FF + \frac{u_1}{R_1(0)}\frac{1}{\lambda^2}F\right]\cdot\lambda\cdot\mathrm{J}_1(\lambda r)\mathrm{d}\lambda \\
& + \frac{P_E}{4\pi}\cos^2\theta\int_0^\infty(-\frac{R_1^*(0)}{u_1}FF + \frac{u_1}{R_1(0)}\frac{1}{\lambda^2}F)\cdot\lambda^2\cdot\mathrm{J}_0(\lambda r)\mathrm{d}\lambda
\end{aligned}
\tag{11}
$$

where F and FF are related to the electric properties of the ionosphere layer (Li, 2015).

● EM attribute parameters

Owing to the complicated relationships between the components and the resistivity, polarizability in equations (5) - (11), the apparent resistivity and apparent polarizability can't be defined like the DC and MT method did, only by near field or far field approximation can the expression of near or far field apparent resistivity be given. This imposes restriction on the data collection area and creates great difficulties in the EM data processing and interpretation. In order to get effective attribute parameters the definition was mainly carried out from two aspects: the whole area numerical definition and the way of complex resistivity method and direct current method. Thus, new methods and techniques of electromagnetic exploration with different characteristics were produced.

Through further study on the numerical algorithms, it has become possible to define the apparent resistivity of the entire space using equations (5) – (11). Many scholars have proposed effective methods of defining parameters based on numerical algorithms. He (2010) defined the apparent resistivity of the whole region based on Equation (7) and proposed the WFEM, which organically unified the "near zone", "transient zone" and "far zone", improved the data distortion in the transient zone, and enabled electromagnetic sounding to be carried out in a vast region without being limited to the far zone. In addition, this definition was also introduced into the LOTEM, MTEM, and WEM, which has resulted in several breakthroughs regarding the data interpretation level and application effect (Yang,1986, Yan, 1999).

On the other hand, referring to the definition methods of apparent resistivity, apparent polarizability and charging rate in CR and DC to directly define the electromagnetic property parameters. According to the characteristics of the simultaneous data acquisition in TFEM, the EM attribute parameters, including the dual-frequency amplitude, dual-frequency phase, triple-frequency phase, and rate of change, were defined as follow:

$$\Delta A(\omega_i) = \frac{A(\omega_i) - A(\omega_{i3})}{A(\omega_i)} \tag{12}$$

$$\Delta\Phi_2(\omega_i) = \frac{\omega_{i3}\Phi(\omega_{i1}) - \omega_i\Phi(\omega_{i3})}{\omega_{i3} - \omega_i} \tag{13}$$

$$\Delta\Phi_3(\omega_i) = \Phi(\omega_i) - \omega\frac{\mathrm{d}\Phi(\omega_i)}{\mathrm{d}\omega} + \frac{2}{3}\omega^2\frac{\mathrm{d}^2\Phi(\omega_i)}{\mathrm{d}\omega^2} \tag{14}$$

$$M_s = \frac{\frac{1}{t_m - t_{m-1}}\int_{t_{m-1}}^{t_m}\varepsilon(t)\mathrm{d}t}{\varepsilon_0} \tag{15}$$

Where ω_{i3} is the 3rd harmonic frequency of the fundamental frequency ω_i; A and Φ represent the amplitude and phase of the fundamental wave, respectively; ε_0 represents the initial potential, t_m and t_{m-1} represent the mth and (m-1)th observation time, respectively; the difference between the t_m and t_{m-1} is the length of the mth observation time window; $\varepsilon(t)$ is the potential decay curve of potential with time t.

The observation mode and the principle of the FSEM were shown in Figure 15. Using equation (5), Davydycheva (2006) defined four EM property parameters using voltages observed at the center of dual sources as follows:

$$\sum_{AB}\frac{\Delta_x U(t)}{\Delta_x U(t_0)}, \quad \sum_{AB}\frac{\Delta_x^2 U(t)}{\Delta_x U(t)}, \quad \sum_{AB}\frac{\Delta_t\Delta_x^2 U(t)}{\Delta_x U(t)}, \quad \sum_{AB}\frac{\Delta_t\Delta_x^2 U(t)}{\Delta_t\Delta_x U(t)} \tag{16}$$

Where

$$\Delta_x U(t) = U_{x2}(t) - U_{x1}(t)$$

$$\Delta_x U^2(t) = (U_{x1}(t) - 2U_{x1}(t) + U_{x3}(t))$$

$$\Delta_t\Delta_x U(t) = \Delta_x U(t + \Delta t) - \Delta_x U(t)$$

$$\Delta_t\Delta_x^2 U(t) = \Delta_x^2 U(t + \Delta t) - \Delta_x^2 U(t)$$

It can be seen from Figure 15 that the FSEM has the characteristic of current vertical focusing, which improves the vertical resolution and the detection depth, and effectively suppresses the interference by the inhomogeneous sub-surface targets.
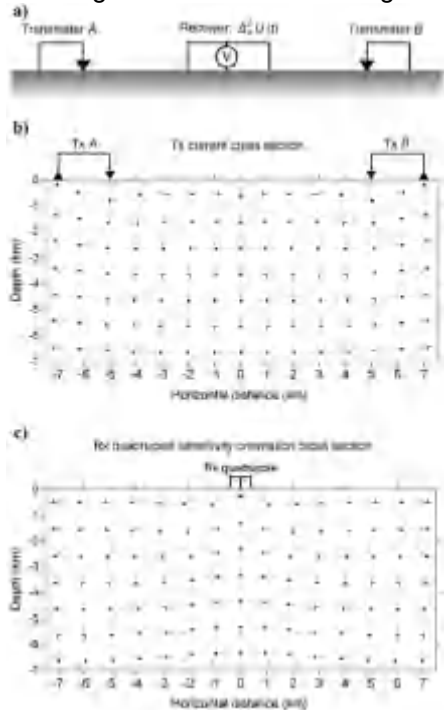

Figure 15. (a) The experimental setup with grounded electrodes (the earth is gray); (b)the dc current pattern for the transmitters, and (c) the receiver. Arrows indicate directions of current flow. The setup provides vertical current focusing. (Davydycheva, 2006)

3.2 Application of the Pseudo-random technique

The auto-correlation of pseudo-random time series (such as M-series) satisfies

$$R_{xx}(\tau) = K\delta(\tau).\tag{17}$$

The cross-correlation between signal and noise satisfies

$$R_{xn}(\tau) = 0 \tag{18}$$

Therefore, the cross-correlation between the earth response and the system input (transmitting signal) is

$$R_{xx}(\tau) = \int_0^{T_s} g(s)\cdot R_{xx}(\tau - s)ds = K\cdot g(\tau) \tag{19}$$

Equation (19) shows that due to the cross-correlation between the wider transmission band M-sequence and the observed EM field components, it is easy to remove the noise and obtain the earth impulse response with a high signal-to-noise ratio. Using the apparent resistivity expression defined by the impulse response of the homogeneous half-space, the apparent resistivity of can be easily calculated (Ou, 2019). In time-domain EM methods, such as the MTEM, WEM, and LowTEM, the pseudo-random technique of M-sequence current

waveform was generally adopted, and thus, the data quality was significantly improved. Moreover, this ensured fast data processing and high-resolution inversion and imaging. Figure 16 and Figure 17 showed the impulse response for the homogeneous earth model obtained from the cross-correlation between the observation field and the pseudo-random MT sequence, which was consistent with the theoretical modeling results.
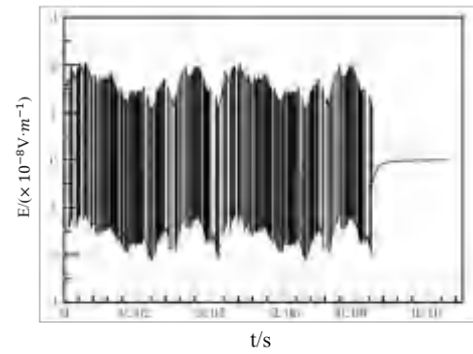

**Figure 16.** the electric fields inspired by the pseudo-random M-sequence.
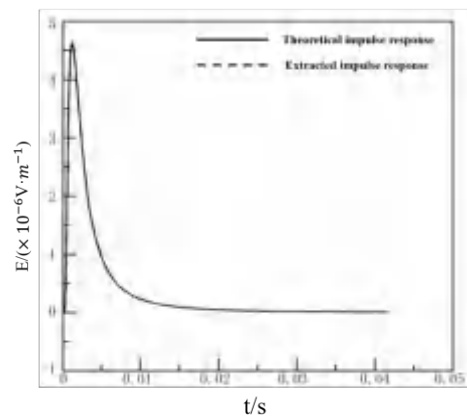
Figure 17. the obtained earth impulse response and the analytical solution.
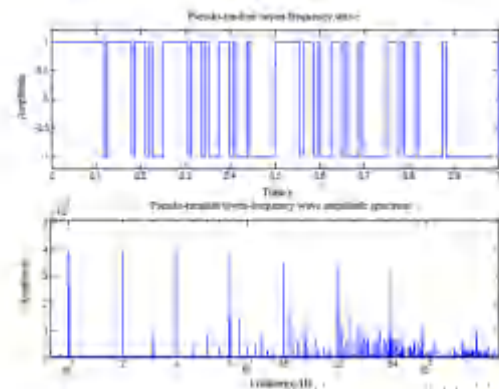

Figure 18. the pseudo-random seven-frequency waveform (A=1, T=1s), the time-domain waveform(top), and the spectrum (bottom, Jiang, 2010)

Another use of pseudo-random is the application of the 2^n sequence. Because the main frequencies of the 2^n sequence waveform are uniformly distributed along the logarithmic coordinate, the amplitudes and initial phases are essentially the same (Jiang, 2010). Using this waveform WFEM improved work efficiency and anti-interference ability, and ensured data quality. For example, the amplitudes and phases of seven frequencies can be obtained at one observation (Figure 18).
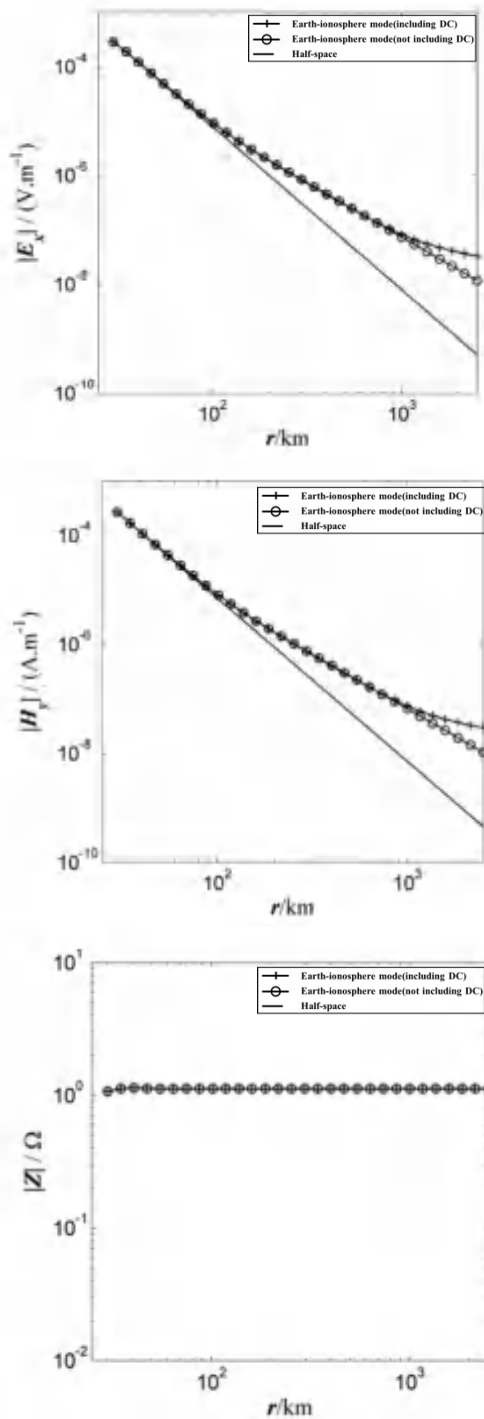

Figure 19. |Ex| (top), |Hy| (middle)and |Z| (bottom) field decay curves for axial array at 32 Hz (Li et al.,2015
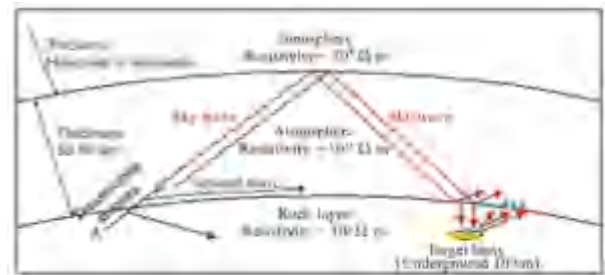
Figure 20. The EM waves propagation of WEM source (Di, 2020).
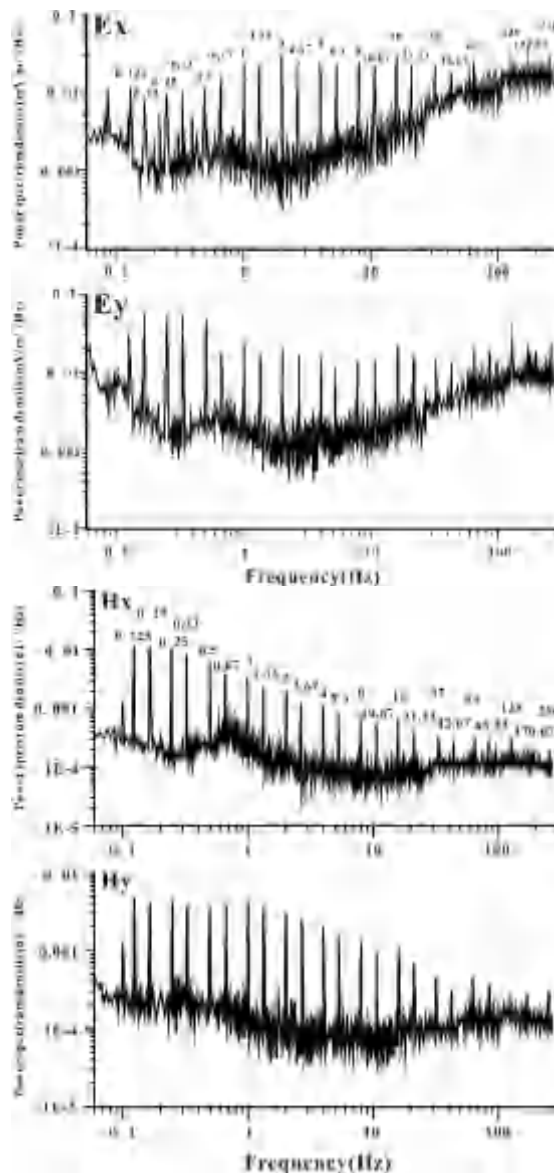
Figure 21. The comparison of power spectral density between WEM and MT fields.

3.3 Utilization of the sky-wave

From the modeling of field components for different lengths of wire source at different frequencies based on equations (6) and (7), Di et al. (2020) found that, when the source length is equal to the

height of the ionosphere, the influence of the sky-wave (wave guide) should be considered. Figure 18 showed that the electric field observed on the ground based on the earth model was significantly larger than that of the homogeneous half-space model when transmitter to receiver distance(r) was more than several hundreds kilometers. Based on this discovery, WEM was proposed by Di et al. (2008) Figure 20 is the principle map of WEM. Since the beginning of this century, China has carried out the research and construction of 'Extremely Low-frequency Ground Exploration Project', and established a fixed tensor source with a scale of over 100 kilometers in Central China, the transmitting power was up to 500kW, 21 frequencies were transmitted, and the frequency band ranged from 0.1Hz to 300Hz. Due to the existence of waveguide field, the WEM signal on the MT background can be observed effectively at far distance (Figure 21). Compared with MT data, the WEM data was considerable superior in quality (Figure 22), which has important theoretical and practical significance for EM exploration in mainland China.
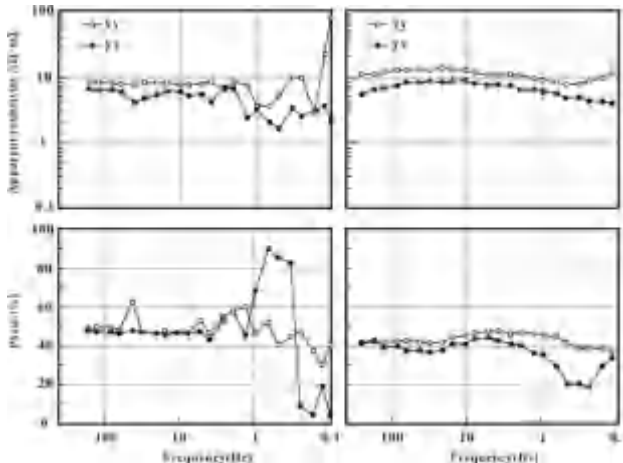

Figure 22. the comparison of apparent resistivity and phase curves between WEM(right) and MT (left)at site 31.

3.4 Reference observation and processing technology of CSEM

In addition to conventionally increasing the current, increasing the number of stacking and increasing the observation time to improve the data signal-to-noise ratio, the application of reference observation and processing technology of CSEM was also the key to ensure the quality of data. Yan (2012) proposed the near-reference magnetic field observation and processing technology for CSAMT. This technique improved the quality of the data by correcting the high-quality magnetic field component data from the near-reference observation and introducing it into the Cagniard apparent resistivity calculation of the CSAMT data of the observed profile. With the increasing
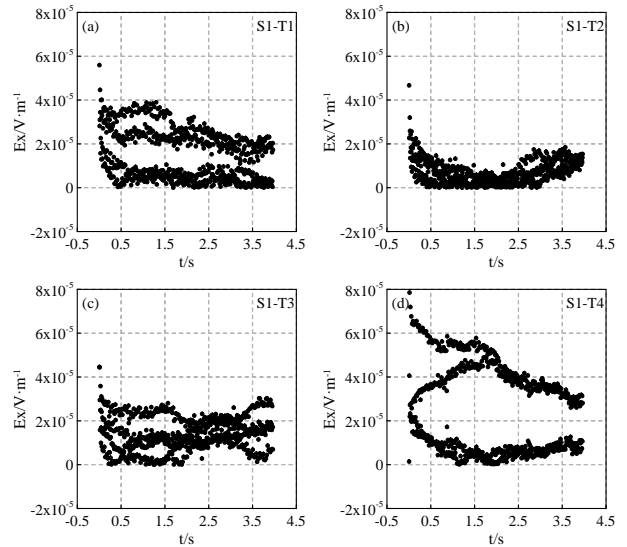

Figure 23. Raw data of 4 periods observed in the suburban area with strong culture noise.
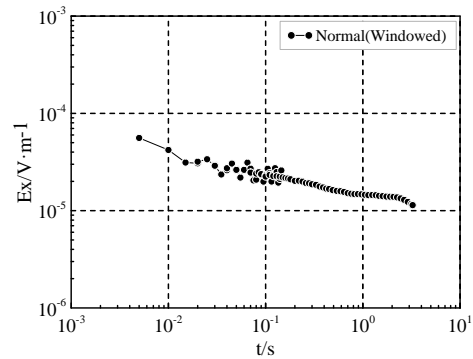

Figure 24. Ex Decay curve with stack and window filtering processing.

popularity of distributed design, array measurement and area data acquisition, the spatiotemporal characteristics of array data provided favorable conditions for reference processing technology. Zhou Cong and Tang Jingtian (2019) proposed a space-time array mixed-field source electromagnetic method (STAHSEM). It was based on multi-input and multi-output system analysis, established a spatiotemporal array equation system using multi-field sources and noise characteristics. By processing the array data synchronously observed by multiple stations, the high quality electromagnetic data of natural field source and controllable source can be obtained while suppressing the relevant noise effectively. In LowTEM data de-noise processing, a method of the local noise compensation (LNC) combined with the variational mode decomposition (VMD) was proposed, which can effectively suppress the noise in the time-domain EM data and improve the decay curve quality. Figure 23 was the LowTEM raw data of four periods observed in the strong cultural noise region. Figure 24 was the Ex decay curve obtained by conventional stacking and filtering. And Figure 25 was the decay curve processed by LNC & VMD.

After comparison, it can be seen that the quality of the head branch of the curve was obviously improved, and the tail branch was more reasonable.
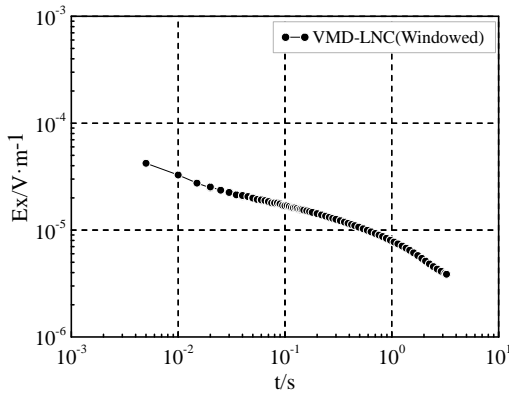

Figure 25. Ex Decay curve with the VMD and LNC joint processing.
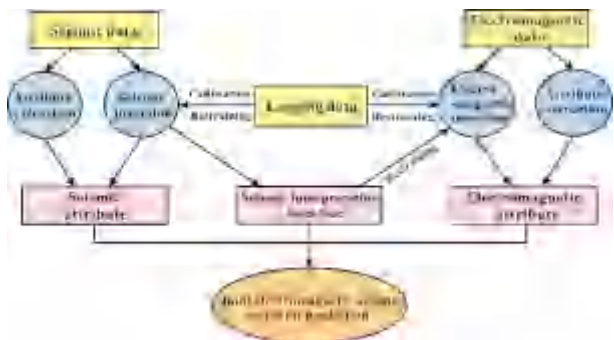
**Figure 26.** TFEM parameter extraction and inversion route with seismic data constraint
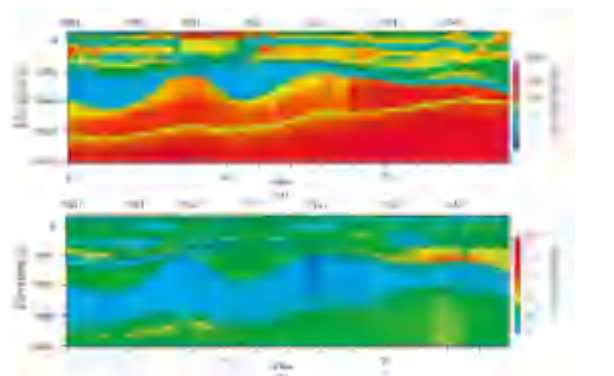
Figure 27. Inversion profile of resistivity and polarizability (top is for resistivity; bottom is for polarizability)

3.5 Joint and constraint data inversion

Various geophysical methods obtain the physical property information from different perspectives. Due to the existence of multiple interpretations in inversion, the different geophysical interpretation methods produce significant differences in the geological models, and even it cannot be reconciled. Joint inversion of multi-methods and multi-

observation fields with the prior information constraints is the most effective way to improve the resolution and reliability (He, 2020, Liu, 2021). He (2020) established a joint objective function through TFEM multi-component data, and proposed a method to constrain parameters spaces of thickness, resistivity, and polarizability using prior seismic information and well loging. They combined the artificial fish and simulated annealing non-linear algorithms and the step-by-step constraint schemes together, which successfully overcame the non-uniqueness of inversion, ensured the exploration accuracy and effect. Figure 26 was the data-constrained inversion route. Figure 27 showed the resistivity and polarizability constrained inversion results of the application in the tight oil and gas exploration. In the inversion process, besides the priori interface information, it was also constrained based on logging and geological information (upper and lower boundaries). From the Figure 27, it can be seen that there existed a variation for resistivity and polarizability in the lateral direction in the same stratum, and the resolution of the thin layer in the vertical direction was significantly improved. Therefore, with more prior information, the inversion was more accurate for the unknown physical parameters.

4. Cases history

MT plays an important role in oil and gas exploration in the basin. At the beginning of this century, with the development of CSEM, this method has been expanded from exploration to development, from oil and gas structure exploration to trap exploration, and to oil and gas detection, and the status of EM method in oil and gas exploration has been rising. As oil and gas exploration moved to unconventional area, the geological and geophysical properties of exploration targets have changed greatly, new exploration fields, such as hydraulic fracturing monitoring of shale gas, tight gas and coalbed methane, and sweet spot detection of shale gas and tight gas, have put forward higher requirements for electromagnetic exploration methods and technologies. MT method did not meet the needs of oil and gas exploration in the strong electromagnetic noise environment. In recent years, with the further research on the geological and electrical characteristics of unconventional oil and gas reservoir, many new CSEM methods and techniques have emerged, and have been used in unconventional oil and gas exploration and development (Zhang, 2013; Zhang, 2017; Yan, 2018; Wang, 2019). In the following, this paper will present three cases on the sweet spot detecting, hydraulic fracturing monitoring and fluid property identification with TFEM, WFEM, and LowTEM methods.

4.1 WFEM application in shale oil and gas exploration

Jiangxi, China, is a province lacking conventional oil and gas resources, but there are several sets of mud shale and oil shale formations such as Cretaceous, Permian, Silurian, Cambrian, etc., which are widely distributed, thick and relatively stable. With the geological conditions for the formation of shale oil and gas reservoirs, shale oil and gas, tight oil and gas resources have great potential and good prospects for exploration and development. A basin to be explored in southern Jiangxi is mostly covered by red layers, developed underground volcanic rocks, and has many small local structures, and the geological and topographical conditions are complex, the shale target layer is generally buried at a depth of about 1500m. In this area sweet spot detection, seismic wave impedance difference was small, reflected energy was weak, seismic wave scattering was serious, and data quality is low. Conventional electromagnetic exploration data acquisition was difficult, and the detection depth and accuracy wee difficult to meet the requirements. To reveal the electrical characteristics and EM response principles for the source rocks in the basin, provide the theoretical basis for the geological evaluation, and determine the location of well drilling, A research group from Central South University carried out the WFEM exploration in this region. It deployed a survey line perpendicular to the structural trend of the basin. In this project, they expected to ascertain the basin structure, basement properties, stratigraphic distribution, and fault characteristics, determine the stratigraphic distribution of the lower Cretaceous Banshi formation for the main target layer, and circle the sweet spots. Table 2 showed the statistical results of stratigraphic lithology and resistivity stratification. From Table 2, we can see that from cover to basement, it can be divided into four electrical layers: the first layer includes sandstone, siltstone, and Mudstone of Guifeng group and Zhoutian formation, showed medium resistivity, and with a thickness of 700m; the second layer included conglomerate, glutenite and siltstone of Maodian, Lengshuiwu formations, showed sub-high resistivity, and with a thickness of about 600m; the third layer included shale, oil shale, and Mudstone of Banshi, showed obvious low resistivity, and with a thickness of about 700m, the fourth layer included limestone and quartz sandstone of Jilongzhang, Linshan formations, and showed high resistivity.

In order to analyze the feasibility of WFEM detection, two models of hydrocarbon-bearing shale (resistivity of 50Ω·m and non-hydrocarbon shale (resistivity of 200Ω·m) of the target layer (the third electric layer) were established according to Table 2 for forward calculation. The blue and red lines in

Figure 28 were the apparent resistivity curves corresponding to the oil-gas shale and the oil-free shale, respectively. There was a significant difference afterward, and the maximum anomaly can reach 60%, which indicated that whether the Banshi formation contained carbonaceous shale can be identified according to the anomaly of the apparent resistivity curve of WFEM. Figure 29 was the pseudo profile of primary apparent resistivity curves formed by the electric field. According to the continuity and lateral variation in this figure, the structures can be qualitatively interpreted. There existed a sharp lateral variation of the curves between site 116 and site 129, which indicated that the structure of this section was complex, and the curve continuity of other sites performed well, which showed a relatively simple structure accordingly.

Table 2. Statistical results of lithology and resistivity for the Banshi formation and its upper and lower strata

Stratum	Main lithology	Resistivity (Ohm-m)	Electrical characteristics
K_2g	Fine sandstone, Sand mudstone, Conglomerate, Cobblestone	100~200	Intermediate resistivity
K_2z	Sandstone, Glutenite, Siltstone, Mudstone	50~300	
K_2m	Conglomerate, Glutenite, Siltstone	230~650	Secondary high resistivity
K_1l	Glutenite, Fine sandstone, Siltstone, Tuffaceous sandstone, Silty mudstone, Mudstone	300~500	
K_1b	Shale, Oil shale, Mud shale, Marl	36~125	Low resistivity
K_1b	Breccia lava, Siltstone, Conglomerate, Tuff	50~470	Intermediate resistivity
K_1j	Rhyolitic brecciated tuff	700~1800	High resistivity
J_1l	Sandstone	1014~2893	

Figure 30 was the profile of the 2D resistivity inversion and geological interpretation. It showed that the resistivity profile can be divided into three sections laterally: the first part was the southeast section (from site 101 to site 126) with the formation resistivity as a high-low-high distribution from top to bottom; the second part was the middle part (from site 126 to site 170) with the formation resistivity as a low-high-low distribution from top to bottom; the third part was the northwest section (from site 170 to site 195) with the formation resistivity as a high-

low-high distribution from top to bottom. In general, the survey line reflected a NE-dipping faulted basin. The strata at both ends of the survey line were uplifted as a whole, and the middle stratum was overall depression. In the depression, there was a wide and gentle anticline in the Cretaceous (from site 126 to site160).
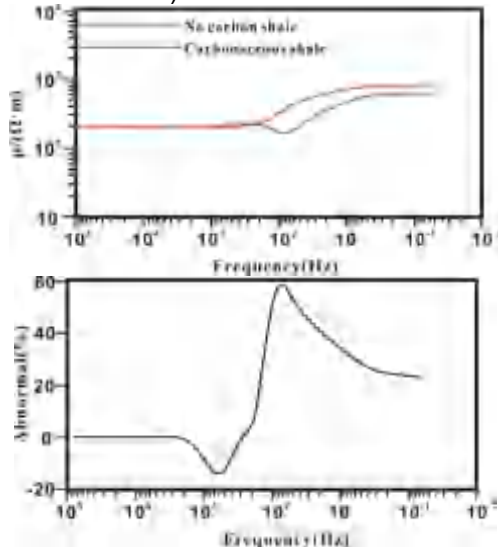

Figure 28. the apparent resistivity and abnormal amplitude curves corresponding to oil-gas and non-oil-gas shales

Figure 29. the primary apparent resistivity curves formed by the electric field for the survey line.
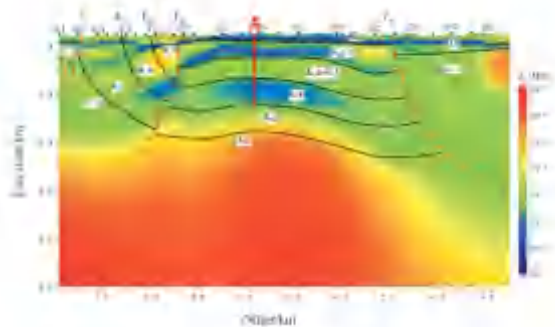
Figure 30. The profile of the 2D resistivity inversion and geological interpretation
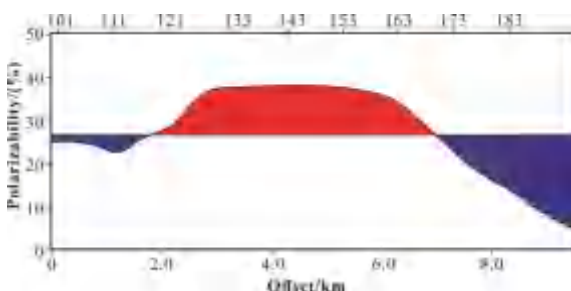

Figure 31. The profile of the polarizability curve

The uplift-in-concave feature in the middle of basin was obvious. The development of fault structure concentrated at the south and north ends of the profile was intense. F70 and F26 were the primary fault zones in the north and south faulted basins, respectively. These two fault zones were reverse faults, and some faults at the southern end of the profile controlled the shale layer. Oil shale, Mudstone, shale and other organic-rich source rocks in the Banshi formation were self-generated and self-stored, which was a favorable reservoir for shale oil and gas.

The fault structure at the middle part of the survey line (from site 126 to site 170) was relatively promising area for oil shale oil development with a deeper target layer depth and a good stratigraphic continuity. Figure 31 is the profile of polarizability curve. It showed that the section from site 116 to site 170 had a high polarized anomaly. Integrated information of resistivity and polarizability the sweet spot can be interpreted in the area between site126 to site 170, with a buried depth of 1000-1600m, an average thickness of 560m. Drilling well 1 is located between site 142 and site 143. Figure 32 is the depth histogram of drilling lithology formation. The buried depths of the bottom of Guifeng, Zhoutian, and Maodian formations were 116m, 466.53m, and 924.46m respectively. The depths of the three interfaces interpreted from the resistivity profile were 155m, 490m, and 920m, respectively. This showed that the inversion depths were very consistent with the drilling results. In addition, the drilling encountered a 2m thick fractured oil-bearing shale in the Banshi formation at a depth of 1500m. This indicated that the inversion depth was accurate, the interface of the electrical layer was clear, and the WFEM it was very sensitive to the conductive oil shale.

Figure 32. The histogram of the drilling stratum, lithology, and resistivity

4.2 TFEM Application in tight oil exploration

PM exploration area in the Middle East has been fully conducted by 3D seismic, with hundreds of oil Wells and abundant geological and geophysical data. However, the seismic method can not solved the distribution of source rocks under the tight reservoirs and deep gypsolytes. TFEM can easily penetrate the high resistivity layers and identify low-resistivity and high-polarization targets. BGP used TFEM to detect sweet spots in the upper and lower layer of the gypsolyte in the PM exploration area.

● The Geo-electrical Model

The main electrical marker layer in this area is a set of gypsolyte layer with a depth of 2000m and a maximum thickness of 1000m, which is partially missing. The seismic exploration have identified undulations in the top interface, the rock formation was characterized clearly by drilling data, and the resistivity was stable, about 2000$\Omega \cdot$m. There are three sets of reservoirs in the exploration area, the main reservoir is clastic reservoir of the upper Paleozoic Khlata Group, the other two are sandstone reservoir of the Safig formation on the top of the lower Paleozoic Ordovician and sandstone reservoir of the Haima group under the plaster rock.

Based on the geological and drilling information, the strata above 3500m depth can be divided into 16 layers, with the 8th layer being the targeted reservoir. The main oil area of this reservoir has been exploited. The resistivities of the water-bearing and oil-bearing reservoirs are 1.5 $\Omega \cdot$m and 200 $\Omega \cdot$m, and the average resistivity is 70 $\Omega \cdot$m. The Lithology and geo-electric model data were shown in Table 3 and Figure 32.
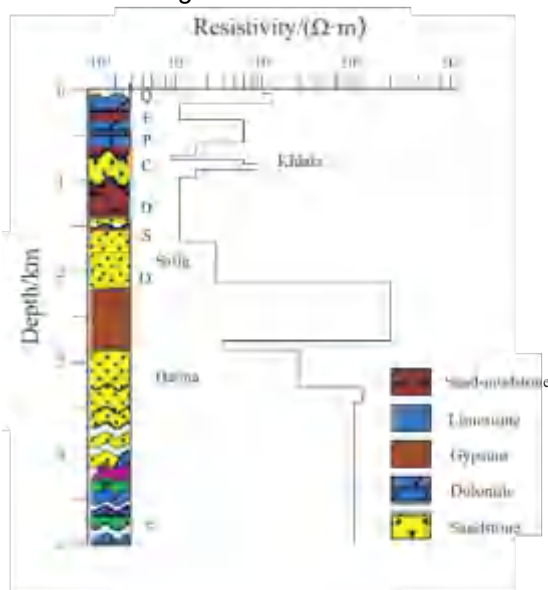

Figure 33. The layered geo-electric model

● Feasibility analysis of the methods

Based on the geo-electric model (Figure 33), and the ranges of the constraint model spaces were used in Table 3. The effectiveness of 1D model space constraint inversion method with artificial fish swarm no-linear algorithm can be tested. Table 4 showed the inverted resistivities. From Figure 33, and Tables 3 and 4, the inversion results were almost consistent with the model, which showed that the artificial fish swarm inversion was correct and feasible.

Layer number	Inversion results ($\Omega \cdot$m)	Theoretical model ($\Omega \cdot$m)
1	85.54	80
2	102.58	100
3	7.94	8
4	49.81	50
5	4.98	5
6	9.61	10
7	25.94	25
8	69.66	70
9	13.59	15
10	20.31	20
11	4.98	5
12	2211.80	2000
13	48.35	50
14	192.45	200
15	537.10	500
16	989.80	1000

Table 4. The inversion results of the electrical parameters

● Interface constrained resistivity inversion

Based on the interpretation results of 3D seismic data in PM exploration area and the well data nearby, a geometric model of formation interface of the survey line was constructed (the dot lines in Figure 35). The model interface was fixed when the TFEM data inversion was conducted, and then the resistivity model (Table 3) was applied in the constraint inversion, and the inversion results were shown in Figure 34. It showed that the resistivity coincided well with the formation interface, the gypsum resistivity coincided with the logging data, and it represented clear interfaces and strong horizontal continuity. In addition, the inversion results presented a clear Carboniferous oil-bearing reservoir (from site 1014 to site 1104). Compared with the drilling data, the interface depth was entirely consistent with the resistivity for each layer. The section from site 1054 to site 1074 was an oil field area that has been exploited for over ten years. Due to the water injection production, the resistivity was generally lower than that of the undeveloped area. The high resistivity anomaly between the site 1094 and site 1154 was quite apparent. Whether it was a favorable sweet spot can be comprehensively judged in combination with the anomaly of polarizability.

● Interface and resistivity joint constrained polarizability inversion

To improve the accuracy of polarizability inversion, an artificial fish swarm inversion with simultaneous constraints of interface geometry model and resistivity model was applied. Table 3 showed the polarizability model and the model space. The polarizability model space for different strata was determined based on the lithology analysis data, but the polarization of the reservoir was not constrained. Figure 34 showed the polarizability inversion profile. The section from site 1014 to site 1104 was the location of the known oil reservoir, it can be seen that the main Carboniferous reservoir had pronounced high polarization characteristics. Combined with the high resistivity characteristics for resistivity profile (Figure 35), the area from the site 1094 to site 1154 was circled as a sweet spot, and the high resistivity and low polarization anomaly near the site 1114 was not. The section of 1154-1184 was also characterized by high polarization and high resistivity, and it was also circled as a sweet spot, this interpretation was confirmed by the drilling results. Hence, joint interpretation of the sweet spot and its distribution area with resistivity and polarization increased the success rate of oil and gas exploration for TFEM.
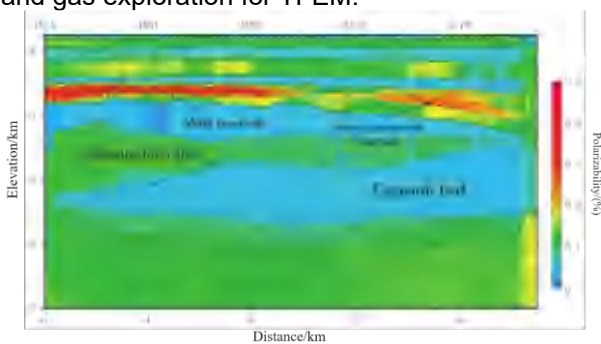

Figure 34. The interface and resistivity model constrained polarizability inversion profile
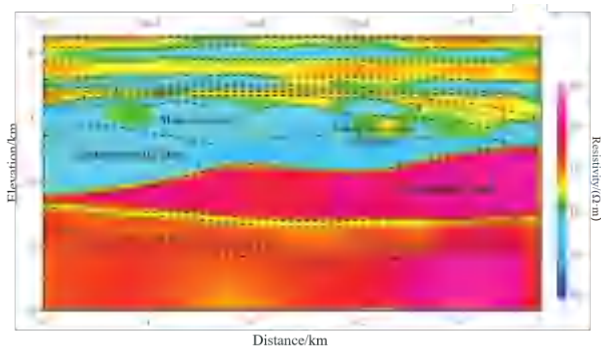

Figure 35. The interface constrained resistivity inversion profile.

4.3 Application in dynamic monitoring of hydraulic fracturing

Jiaoshiba shale gas field is the largest integrated gas reservoir in China. The effective application of hydraulic fracturing technology is conducive to stabilizing and increasing production in this area.

Micro-seismic monitoring plays a vital role in improving the fracturing effect. However, affected by the complex terrain and surface geological conditions in southern China, the signal-to-noise ratio of micro-seismic monitoring was low, and the positioning accuracy was not high. In addition, limited by the micro-seismic method, the estimation of effective volume (ERV) is not accurate very much (Hoversten,，2015). It is well known that when a large amount of fracturing fluid is injected into the reservoir rock, it will flow along the microfractures and continuously expand the fractures, this leads to the change of electrical properties. Due to the low resistivity characteristics of the fracturing fluid and the good connectivity caused by fracturing fluids, the stimulated reservoirs show good low resistivity and high polarizability characteristics, therefore, EM fracturing monitoring has a good physical property foundation. The application of EM methods can obtain sensitive parameters such as fluid trend, volume change and connectivity during the fracturing process, so as to achieve the purpose of monitoring in unconventional oil and gas reservoir fracturing.

In 2017, the EMLAB group of Yangtze University applied the LowTEM method to conduct continuous time-domain EM fracturing monitoring test in Jiaoshiba shale gas field. Through 224 Ex channels of data acquisition array, nearly 9 hours Ex component time series data had been acquired over three fracturing stages buried at a depth of 2800 meters. Through 4D LowTEM processing, the sensitive parameters of electrical changes caused by the fracturing of shale reservoirs were obtained, and the spatial distribution of the fracturing fluid was imaged. The results have guiding significance for fracturing production and well pattern adjustment.

● Electric characteristics of stratum

Table 5 showed the parameters the geo-electric model in test area based on JIAOYE #1 well logging. The model showed a good correspondence between resistivity and stratum, and the shale resistivity is obviously lower than that of the surrounding rocks.

● Electrical characteristics of fracturing fluid

Fracture liquids were sampled from three horizontal platforms (The base fluid is 2% potassium chloride). The measured complex resistivity results (Figure 36) showed that there were specific differences in the resistivity amplitude of fracturing fluids on different platforms, ranging from 0.8-6.4Ω·m. Still, they were all about an order of magnitude smaller than shales. The phase showed that they had different minimum values at frequency 50-500Hz, which indicated that they had strong polarization characteristics due to the presence of proppant.

● Normalized residual time-lapse imaging

All-time apparent resistivity was calculated from electric field components observed before and after

fracturing, then resistivity imaging was carried out based on the theory of chimney effect of current diffusion. To highlight the changing of resistivity caused by fracturing, a normalized residual processing method was developed in the log-log domain. The formula is

$$DF_\rho = 100 \times d \, | \log \rho_1 - \log \rho_2 \, | \, / d \log \, h \qquad (20)$$

Where DF_ρ is the value of normalized residual, ρ_1 is imaged resistivity before fracturing, ρ_2 is imaged resistivity after fracturing, and *h* is the depth.
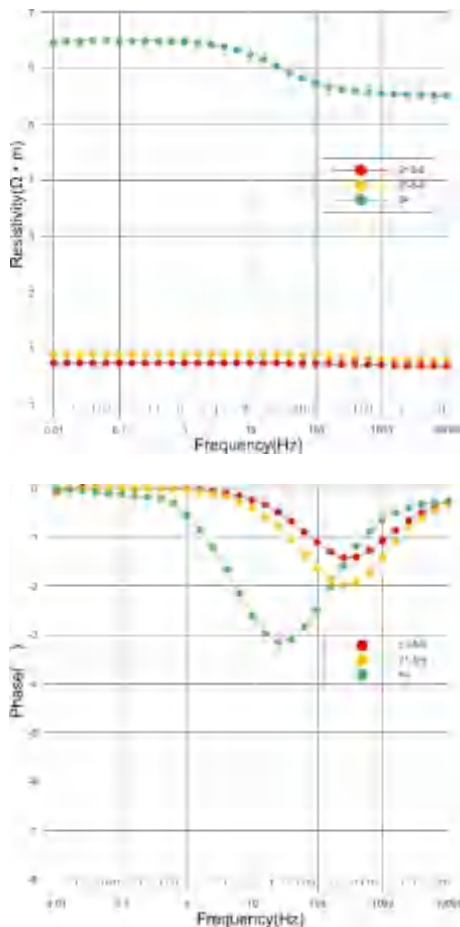
Figure 36. The complex resistivity of fracture liquid (Top: Amplitude; Bottom: Phase)

- Model testing

In geo-electric model(table 5), the resistivity of the reservoir stratum was assumed as 42Ω·m before fracturing, and 5Ω·m after fracturing. The normalized Ex and the normalized residual curves had shown in Figure 37. The top curve showed that the change was identified from decay time 5ms to 100ms when the reservoir stratum fracturing was conducted in the depth of 2330m. Normalized residual curve can depict the fracture change clearly in the range from 30ms to 40ms (bottom curve).

- LowTEM monitoring and analyzing

8 lines with length of 1400m each, 224 sites with 50m interval, were setup above the stage of 6, 7, 8 of the horizontal hydraulic fractured well. The

length of the ground source was 4000m, in an east-west direction, the minimum offset was 5000m, the current was 65A, the current waveform was a bipolar square wave with a period of 8s and a duty cycle of 50%, the sampling rate was 400Hz. The schematic diagram of the field construction layout was shown in Figure 38.
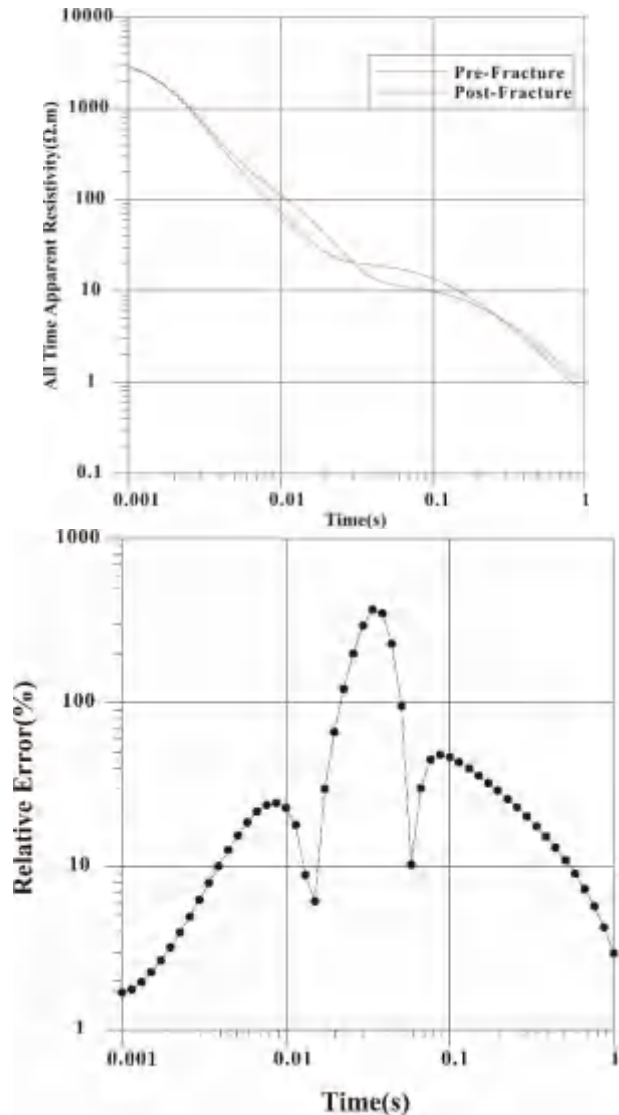

**Figure 37.** The EM field (top) and normalized residual (bottom) curves
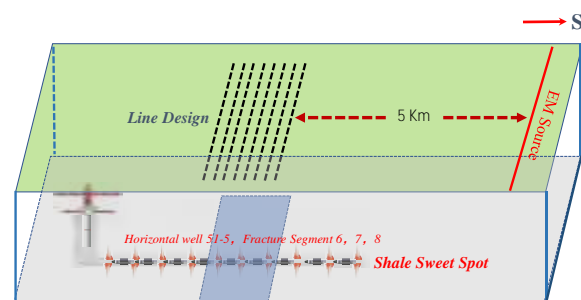
Figure 38. LowTEM Layout for the monitoring of shale fracture

The fracturing production information in the monitoring section is shown in Table. The continuous recording time of Ex while stage 6,7,8 were fractured was up to 9 hours, which ensured the whole process of the fracturing process of each stage. In order to guarantee the quality of decay curve, 30 minutes of electric field component time serious of segment 6, 7, 8 each was used to stack processing, and the normalized residual curves had been acquired on the sites of L01-14 and L01-16. In Figure 39, the weak changes of fracturing can be seen in the decay time range from 0.03s to 0.1s. The shape and time window were consistent with the forward results in Figure 37.
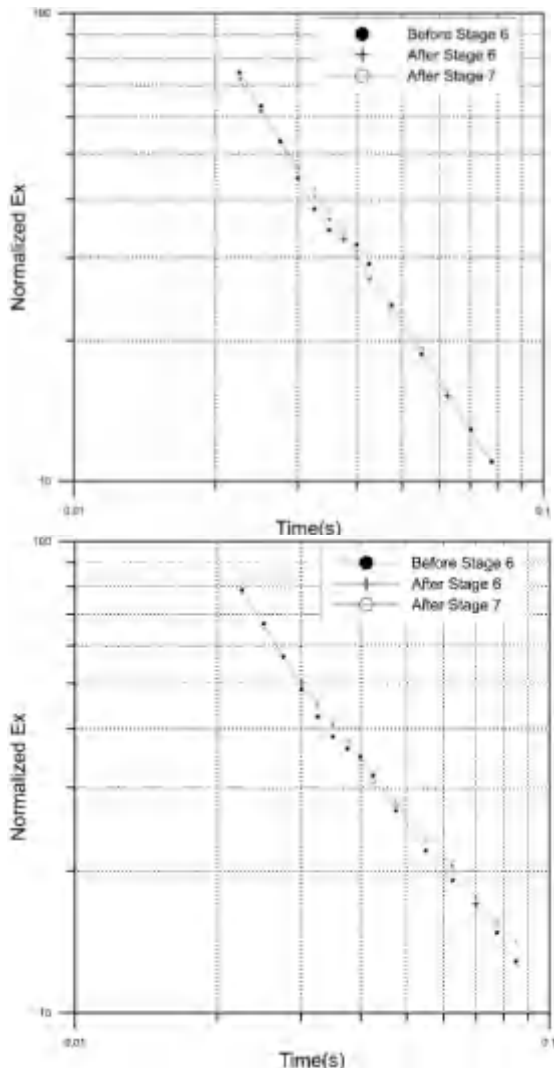

Figure 39. The curves of electric field component Ex observed at points 14 (top) and 16 (bottom) of L01 over the segment 6 and 7 in horizontal wells

The 3D fracturing anomalies showed in Figure 40 which were imaged based on the normalized residual curves, and at the same time the calibration was carried out with the help of seismic and well logging. The results showed that, after segment 6 fracturing the length of the fractured reservoir stratum in the direction of east to west was about

600 m, in which 400m was in the west of horizontal well, 200m was in the east of horizontal well. The width from north to south was about 200-300m. After segment 7 fracturing the length of the fractured reservoir stratum in the direction of east to west was about 700m, in which 400m was in the west of horizontal well, 300m was in the east of horizontal well. The width from north to south increased to 300-400m. Overall, the trend and spatial distribution of fracturing fluid were dumbbell-shaped, and the fracturing effect in the west area was better than that in the east area.
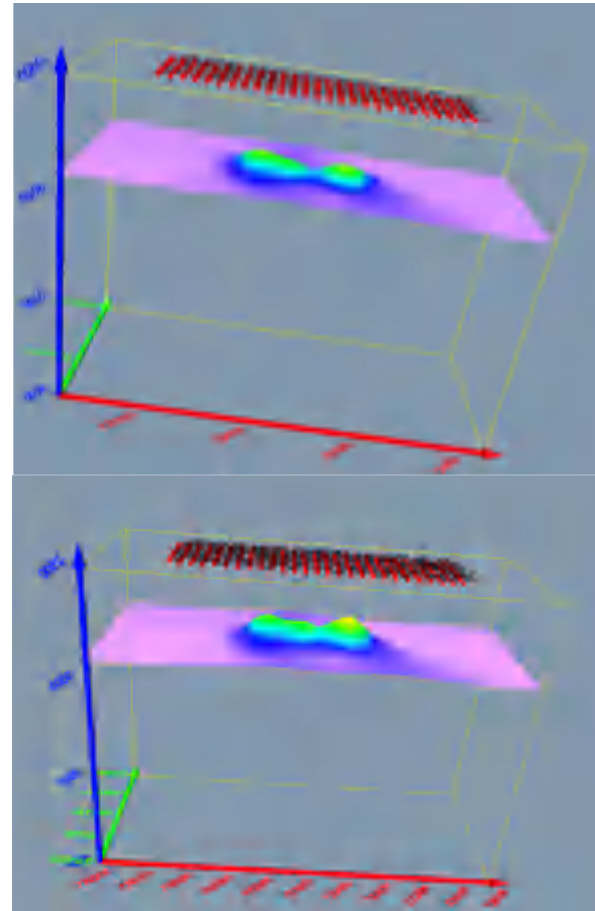

Figure 40. Anomaly in the space before and after fracture(top：after segment 6；bottom：after segment 7)

5 Conclusion and future

5.1 Conclusion

(a) The complex resistivity analysis of reservoir rocks showed that the organic-rich shale in southern China had the characteristics of low resistivity and high polarization. Tight oil and gas reservoirs were characterized by the high resistivity and high polarization. The hydraulic fracturing reservoir stimulation area had the characteristics of low resistance and high polarization. All these indicated that the CSEM detecting the sweet spots had a firm petrophysical basis.

(b) The high spatiotemporal density data collection, combining with updated methods, such as the high-power transmitters, pseudo-random waveforms, reference observation and processing, variational mode decomposition, have improved signal-to-noise ratio and guaranteed data quality, which can profit the accurate inversion.

(c) The new EM attribute parameter definitions greatly improved the sensitivity of CSEM to detect the target attribute and the fluid property, and also facilitated geological interpretation.

(d) With the prior information constraints, such as geology, seismicity, and well logging, the joint inversion of for multiple methods and multiple component data, can produce an accurate and reliable interpretation model.

(e) The sweet spot detection model and the parameter prediction method formed by the EM characteristics of shale reservoirs have laid a physical foundation for applying EM methods in geological evaluation. This techniques can be used for reference in the data interpretation of EM detection in other unconventional reservoirs.

5.2 Future

(a) Research on the inversion method based on IP model under seismic, logging and other prior information constraints should be carried out so that to improve the resolution and reliability of TDEM in unconventional oil and gas exploration.

(b) At present, the application of WEM method has played an essential role in engineering geology, mineral exploration, disaster prevention, and environmental governance. As the WEM source is improved further，it has become a dedicated fixed source that can transmit multi-segment frequency codes, which has improved exploration efficiency, reduced production costs, and ensured effective exploration depths up to 5km. the WEM method has become an essential means in the exploration and development of unconventional oil.

(c) The data collection methods should be continuously optimized. The EM forward model, analysis, and acquisition parameter evaluation before field work are the key to the success of EM survey. Softwires should be developed for EM data collection method and parameter optimization, further to provide robust means for data collection.

(d) The heterogeneity and electrical anisotropy of unconventional oil and gas reservoirs and hydraulic fracturing areas are pretty severe, which will lead to the misunderstandings in data processing and interpretation. It is an unavoidable problem to study the high-precision anisotropy forward modeling and inversion method.

(e) Based on the characteristics of EM exploration and micro-seismic monitoring, an acquisition array system that can simultaneously collect controlled-source EM methods and micro-seismic signals should be developed, effectively achieve the deep integration of EM and micro-seismic in all directions, and form a hydraulic fracturing controlled-source EM method and micros-seismic joint monitoring method.

(f) When we are faced with the difficulty of effectively suppressing the electromagnetic noise, the time-consuming and multi-resolution of 3D inversion, and the unsatisfactory application effect of sweet spot detection and evaluation, the arrival of artificial intelligence and big data show us a new hope. Through big data analysis, we are expected to find the real laws of the noise world, the model world and the underground electrical world hidden behind the big data of electromagnetic exploration. The analysis and prediction of big data through artificial intelligence and cloud computing will make the EM processing and interpretation more accurate, convenient and efficient, thus mining more hidden value of electromagnetic data.

Acknowledgements

References

Archie GE (1942) The electrical resistivity log as an aid in determining some reservoir characteristics. Transactions of the AIME 146(01): 54–62

Astic T, Oldenburg DW (2019) A framework for petrophysically and geologically guided geophysical inversion using a dynamic Gaussian mixture model prior. Geophysical Journal International 219(3): 1989–2012. doi:10.1093/gji/ggz389

Börner FD, Schopper JR, Weller A (1996) Evaluation of transport and storage properties in the soil and groundwater zone from induced polarization measurements. Geophysical Prospecting 44: 583–601

Burtman V, Zhdanov MS, Fu H (2014) Spectral induced polarization effect in unconventional reservoir rocks. SEG Technical Program Expanded Abstracts 33: 907–911. doi:10.1190/segam2014-0419.1

Burtman V, Zhdanov MS (2015) Induced polarization effect in reservoir rocks and its modeling based on generalized effective-medium theory. Resource-Efficient

Technologies 1(1): 34–48. doi:10.1016/j.reffit.2015.06.008

Chen Benchi, Li Jinming, Zhou Fengtong (1999) Quasi wave equation migration of transient electromagnetic field. Oil Geophysical Prospecting 34(5): 546–554

Chen Feng, Xiu Jigang, An Jinzhen (2000) Research on dependence of resistivity changing anisotropy on microcracks extending in rock with experiment. Acta Seismiological Sinica 22(3): 310–318

Commer M, Newman GA, Williams KH (2011) 3D induced-polarization data inversion for complex resistivity. Geophysics 76(3): F157–F171. doi:10.1190/1.3560156

Constable S (2010) Ten years of marine CSEM for hydrocarbon exploration. Geophysics 75(5): 75A67–75A81. doi:10.1190/1.3483451

Davydycheva S, Rykhlinski N, Legeido P (2006) Electrical-prospecting method for hydrocarbon search using the induced-polarization effect. Geophysics 71(4): G179–G189. doi:10.1190/1.2217367

De Lima OAL, Niwas S (2000) Estimation of hydraulic parameters of shaly sandstone aquifers from geoelectrical measurements. Journal of Hydrology 235(1-2): 12–26

Di Qingyun, Wang Miaoyue, Wang Ruo et al (2008) Study of the long bipole and large power electromagnetic field. Chinese Journal of Geophysics (in Chinese) 51(6): 1917–1928

Di Qingyun, Xue Guoqiang, Yin Changchun et al (2020) New Methods of controlled-source electromagnetic detection in China. Scientia Sinica (Terrae) 50(09): 1219–1227

Di Qingyun, Zhu Rixiang, Xue Guoqiang et al (2019) New development of the Electromagnetic (EM) methods for deep exploration. Chinese Journal of Geophysics (in Chinese) 62(6): 2128–2138

Fiandaca G, Auken E, Christiansen AV et al (2012) Time-domain-induced polarization: Full-decay forward modeling and 1D laterally constrained inversion of Cole-Cole parameters. Geophysics 77(3): E213–E225. doi:10.1190/geo2011-0217.1

Gallardo LA, Meju MA (2003) Characterization of heterogeneous near-surface materials by joint 2D inversion of dc resistivity and seismic data. Geophysical Research Letters 30: 1658. doi:10.1029/2003GL017370

Gallardo LA, Meju MA (2004) Joint two-dimensional DC resistivity and seismic travel time version with cross-gradients constraints. Journal of Geophysical Research: Solid Earth 109: B03311. doi:10.1029/2003jb002716

Gao Ji, Zhang Haijiang, Fang Hongjian, Li Nan (2017) An efficient joint inversion strategy for 3D seismic travel time and DC resistivity data based on cross-gradient structure constraint.

Chinese Journal of Geophysics (in Chinese) 60(9): 3628–3641. doi:10.6038/cjg20170927

Giraud J, Pakyuz-Charrier E, Jessell M et al (2017) Uncertainty reduction in joint inversion using geologically conditioned petrophysical constraints. Geophysics 82(6): 1–61. doi:10.1190/geo2016-0615.1

Goldstein MA et al (1975) Audio-frequency magnetotellurics with a grounded electric dipole source. Geophysics 40(1): 669–683

Haber E, Oldenburg DW (1997) Joint inversion: a structural approach. Inverse Problems 13(1): 63–77. doi:10.1088/0266-5611/13/1/006

Heincke B, Jegen M, Moorkamp M et al (2010) Adaptive coupling strategy for simultaneous joint inversions that use petrophysical information as constraints. SEG Technical Program Expanded Abstracts. doi:10.1190/1.3513426

He Jishan (2010) Wide field electromagnetic sounding methods. Journal of Central South University (Science and Technology) 41(3):1065–1072

He Zhanxiang (2019) Opportunities,challenges and development directions of electromagnetic exploration today. Computing Techniques for Geophysical and Geochemical Exploration 41(4): 433–447

He Zhanxiang, Dong Weibin, Zhao Guo et al (2021) Time-frequency electromagnetic (TFEM) technology: Data processing. Oil Geophysical Prospecting 56(6): 1391–1399

He Zhangxiang, Hu Wenbao, DongWeidong (2010) Petroleum electromagnetic prospecting advances and case studies in china. Surveys in Geophysics 31(2): 207–224 doi:10.1007/s10712-009-9093-z

He Zhanxiang, Hu Zuzhi, Gao Yan et al (2015) Field test of monitoring gas reservoir development using time-lapse continuous electromagnetic profile method. Geophysics 80(2): 127–134. doi:10.1190/geo2014-0195.1

He Zhanxiang, Hu Zuzhi, Luo Weifeng, Wang Caifu (2010b) Mapping reservoirs based on resistivity and induced polarization derived from continuous 3D magnetotelluric profiling: Case study from Qaidam Basin, China. Geophysics 75(1): B25–B33. doi:10.1190/1.3279125

He Zhanxiang, Hu Zuzhi, Wang Zhigang (2020) Time-frequency electromagnetic(TFEM) technique: step-by-step constraint inversion based on artificial fish swarm algorithm. Oil Geophysical Prospecting 55(4): 898–905.

He Zhanxiang, Liu Xuejun, Qiu Weiting et al (2005) Mapping reservoir boundary by borehole-surface TFEM: Two case studies. The Leading Edge 24(9): 896–900. doi:10.1190/1.2056379

He Zhanxiang, Wang Xuben (2007) Geo-electrical anomalous pattern of reservoir and oil/gas detection by electromagnetic survey. Oil

Geophysical Prospecting 42(1): 102–106

Hobbs BA et al (2006) Multi-Transient Electromagnetics (MTEM) -controlled source equipment for subsurface resistivity investigation. 18th IAGA WG 1.2 Workshop on Electromagnetic Induction in the Earth. El Vendrell, Spain 17–23

Hoversten GM, Commer M, Haber E et al (2015) Hydro-frac monitoring using ground time-domain electromagnetics. Geophysical Prospecting 63(6): 1508–1526. doi:10.1111/1365-2478.12300

Hu Wenbao, Shen Jingshong, Yan Liangjun (2022) Reservoir Fluid Prediction Theory with CSEM and Application. Science Publish House, Beijing

Hu Wenyi, Abubakar A, Habashy TM (2009) Joint electromagnetic and seismic inversion using structural constraints. Geophysics 74(6): R99–R109

Hu Zuzhi, Shi Yanling, Liu Yunxiang et al (2020) Nonlinear constrained joint inversion of MT and gravity. Oil Geophysical Prospecting 55(01): 1110–1116

Jegen MD, Hobbs RW, Tarits P et al (2009) Joint inversion of marine magnetotelluric and gravity data incorporating seismic constraints: Preliminary results of sub-basalt imaging off the Faroe Shelf. Earth and Planetary Science Letters 282(1): 47–55. doi:10.1016/j.epsl.2009.02.018

Ji Yanju et al (2016) Noise reduction of time domain electromagnetic data: application of a combined wavelet denoising method. Radio Science 51(6): 680–689

Jiang qiyun (2010) Study on the key technology of wide field electromagnetic sounding instrument. PhD thesis, Central South University

Kavian M, Slob EC, Mulder WA (2012) A new empirical complex electrical resistivity model. Geophysics 77(3): E185–E191. doi:10.1190/geo2011-0315.1

Kass MA, Li Y (2011) Quantitative analysis and interpretation of transient electromagnetic data via principal component analysis. IEEE Transactions on Geoscience & Remote Sensing 50(5): 1910–1918

Kirkby A, Heinson G, Krieger L (2016) Relating permeability and electrical resistivity in fractures using random resistor network models. Journal of Geophysical Research: Solid Earth 121(3): 1546–1564

Lelievre PG, Farquharson CG, Hurich CA (2012) Joint inversion of seismic travel times and gravity data on unstructured grids with application to mineral exploration. Geophysics 77(1): K1–K15

Lelievre PG, Farquharson CG (2013) Gradient and smoothness regularization operators for geophysical inversion on unstructured meshes. Geophysical Journal International 195: 330–341. doi:10.1093/gji/ggt255

Li Diquan, Di Qingyun, Wang Miaoyue, David Nobes (2015) 'Earth–ionosphere' mode controlled source electromagnetic method. Geophysics 202: 1848–1858. doi: 10.1093/gji/ggv256

Lima OD, Sharma MM (1992) A generalized Maxwell-Wagner theory for membrane polarization in shaly sands. Geophysics 57(3): 431–440. doi:10.1190/1.1443257

Li Xiu, Xue Guoqiang, Song Jianping et al (2005) An optimize method for transient electromagnetic field-wave field conversion. Chinese Journal of Geophysics (in Chinese) 48(5): 1185–1190

Liu Jianxin, Guo Tianyu, Wang Bochen et al (2021) Review of marine electromagnetic methods for hydrocarbon exploration. Geophysical Prospecting for Petroleum 60(4): 527–538

Mittet, R (2015) Seismic wave propagation concepts applied to the Interpretation of marine controlled-source electromagnetic: Geophysics 80(2) E63–E81. doi:10.1190/geo2014-0215.1

Mittet, R (2018) Electromagnetic modeling of induced polarization with the fictitious wave domain method. SEG Technical Program Expanded Abstracts. doi:10.1190/segam2018-2994774.1

Ou Yangtao et al (2019) Identifying deep ore bodies using the Multi-Channel Transient Electromagnetic Method (MTEM): an example of a lead-zinc-silver mine in Inner Mongolia. Chinese J. Geophys (in Chinese) 62(5): 1981–1990

Pelton W, Ward S, Hallof P et al (1978) Mineral discrimination and removal of inductive coupling with multifrequency IP. Geophysics 43(3): 588–609

Peng Guomin, Liu Zhan (2020) An overview of joint electromagnetic-seismic inversion and its future development. Oil Geophysical Prospecting 55(2): 465–474

Peng Guomin, Xu Kaijun, Du Runlin, Liu Zhan (2018) Reservoir petrophysical parameter estimation with joint inversion of MCSEM and seismic AVA data. Oil Geophysical Prospecting 53(05): 1110–1116

Piao Huarong (1990) Principle of Electromagnetic Sounding. Geological Press, Beijing: Geological Publishing House

Rasmussen S, Nyboe NS, Mai S, Juul Larsen J (2017) Extraction and use of noise models from transient electromagnetic data. Geophysics 83(1): E37–E46.

Revil A, Abdel Aal GZ, Atekwana EA et al (2015) Induced polarization response of porous media with metallic particles—Part 2: Comparison with a broad database of experimental data. Geophysics 80(5): D539–D552. doi:10.1190/geo2014-0578.1

Revil A, Eppehimer J, Skold M et al (2013) Low-frequency complex conductivity of sandy and clayey materials. Journal of Colloid and Interface Science 398: 193–209. doi:10.1016/j.jcis.2013.01.015

Revil A, Woodruff WF, Torres-Verdin C et al (2013) Complex conductivity tensor of anisotropic hydrocarbon-bearing shales and mudrocks. Geophysics 78(6): D403–D418. doi:10.1190/geo2013-0100.1

Seigel HO, Nabighian M et al (2007) The early history of the induced polarization method. The Leading Edge 26(3): 312–321

Slater, L (2007) Near Surface Electrical Characterization of Hydraulic Conductivity: From Petrophysical Properties to Aquifer Geometries—A Review. Surveys in Geophysics, 28(2-3): 169–197. doi:10.1007/s10712-007-9022-y

Slater L, Lesmes DP (2002) Electrical-hydraulic relationships observed for unconsolidated sediments. Water Resources Research 38(10): 31–1–31–13. doi:10.1029/2001wr001075

Stoffa PL, Ziolkowski A (2018) Time evolution of the electric field – Part 1: using the rapid expansion method (REM) with pseudo-spectral evaluation of spatial derivatives. SEG Technical Program Expanded Abstracts. doi:10.1190/segam2018-2995831.1

Strack, KM (2013) Future Directions of Electromagnetic Methods for Hydrocarbon Applications. Surveys in Geophysics 35(1):157–177. doi:10.1007/s10712-013-9237-z

Strack KM (2014) Future Directions of Electromagnetic Methods for Hydrocarbon Applications. Surveys in Geophysics 35:157–177

Strack KM et al (1989) Case histories of long-offset transient electromagnetic (LOTEM) in hydrocarbon prospective areas. First Break 7(12): 467–477

Streich R (2015) Controlled-Source Electromagnetic Approaches for Hydrocarbon Exploration and Monitoring on Land. Surveys in Geophysics 37(1): 47–80. doi:10.1007/s10712-015-9336-0

Streich R, Becken M, Matzander U, Ritter O (2011) Strategies for land-based controlled-source electromagnetic surveying in high-noise regions. The Leading Edge 30(10): 1174–1181. doi:10.1190/1.3657078

Su Zhuliu et al (2005) Appliacation of complex apparent resistivity (CR) method in prediction of oil/gas. Oil Geophysical Prospecting 40(4):467–471

Tietze K, Grayver A, Streich R et al (2014) Developments for Land-based Controlled-source Electromagnetic Surveying. Conference Proceedings, 76th EAGE Conference and Exhibition - Workshops. doi:10.3997/2214-4609.20140561

Tong, Xiaolong, Yan Liangjun, Xiang Kui (2020) Modifying the Generalized Effective-medium Theory of Induced Polarization Model in Compacted Rocks. Geophysics 85(4): 1–44

Veeken PC, Legeydo PJ, Davidenko YA et al (2009) Benefits of the induced polarization geoelectric method to hydrocarbon exploration. Geophysics 74(2): B47–B59. doi:10.1190/1.3076607

Vinegar HJ, Waxman MH (1984) Induced polarization of shaly sands. Geophysics 49(8): 1267–1287. doi:10.1190/1.1441755

Wang Mingfei, Chen Chao, Qu Dapeng et al (2015) The geophysical characteristics of shale gas reservoir from Wufeng member to Longmaxi member in Jiaoshiba block of Fulin shale gasfield. Geophysical Prospecting for Petroleum 54(5): 613–620

Wang Zhigang et al (2019) The use of time-frequency domain EM technique to monitor hydraulic fracturing. GEM 2019 Xi'an: International Workshop and Gravity, Electrical & Magnetic Methods and their Applications

Weller A, Slater L, Binley A et al (2015) Permeability prediction based on induced polarization: Insights from measurements on sandstone and unconsolidated samples spanning a wide permeability range. Geophysics 80(2): D161–D173. doi:10.1190/geo2014-0368.1

Wong J (1979) An electrochemical model of the induced-polarization phenomenon in disseminated sulfide ores. Geophysics 44(7): 1245–1265.doi:10.1190/1.1441005

Wu Changxiang et al (1996) The applleation of complex resistivity method in oil field exploration. Geophysical Prospecting for Petrole 35(4): 111–118

Wu Sihong, Huang Qinghua, Zhao Li (2021) De-noising of transient electromagnetic data based on the long short-term memory-autoencoder. Geophysical Journal International. doi:10.1093/gji/ggaa424

Xiang Kui, Hu Wenbao, Yan Liangjun et al (2014) Complex resistivity dispersion characteristics of shale samples in Sichuan and Guizhou area. Oil Geophysical Prospecting 49(5): 1013–1019

Xiang Kui, Yan Liangjun, Hu Hua, Hu Wenbao, Tang Xingong, Liu Xuejun (2016) Relationship analysis between brittle index and electrical properties of marine shale in South China. Geophysical Prospecting for Petroleum 55(6): 894–903

Xu Chuanjian et al (2004) Application effectiveness of complex resistivity (CR) method in oil and gas   detection. Oil Geophysical Prospecting 39(S1): 31–35

Xu Fengjiao, Yan Liangjun, Xiang Kui et al (2020) Predicting the characteristic parameters of

shale sweet-spot with complex resistivity. Terrestrial, Atmospheric and Oceanic Sciences journal. doi: 10.3319/TAO.2020.03.22.01.

Xu Kaijun, Du Runlin, Liu Zhan (2016) Joint reservoir parameter inversion of 1D marine controlled source electromagnetic and seismic data. Oil Geophysical Prospecting 51(01): 197–203

Xue Guoqiang, Chen Weiying, Wu Xin (2020) Review on research of short-offset transient electromagnetic method. Journal of China University of Mining & Technology 49(2): 215–226

Xue Guoqiang, DI Qingyun, Wang Ruo et al (2020) Overview on data processing methods of multi-channel transient electromagnetic method. Progress in Geophysics (in Chinese) 35(1): 0211–0215

Xue Guoqiang, Wu Xin, Li Hai et al (2016) Progress of multi-transient electromagnetic method in abroad. Progress in Geophysics (in Chinese) 31(5): 2187–2191

Yan Liangjun, Hu Wenbao (1999) The estimation and fast inversion of All-time apparent resistivity for LOTEM. Oil Geophysical Prospecting 34(5): 532–538

Yan Liangjun (2014) Study on the induced polarization model in the exploration for shale gas in southern China. SEG Technical Program Expanded Abstracts. doi:10.1190/segam2014-0186.1

Yan LiangJun, Chen Xiaoxiong, Tang Hao et al (2018) Continuous TDEM for monitoring shale hydraulic fracturing. Applied Geophysics 15(1): 26–34. doi:10.1007/s11770-018-0661-1

Yan Liangjun et al (2012) Magnetic reference technique and correction method in 3D CSAMT. SEG Technical Program Expanded Abstracts. doi:10.1190/segam2012-0239.1

Yang Bo, Zhang Xiangguo, Liu Zhan, Xu Kaijun (2021) Technique and application of joint magnetotelluric and seismic modelling and constrained inversion based on clustering and multiviariate geostatistics. Oil Geophysical Prospecting 56(03): 670–677

Yang Chunmei, LI Hongqi, Zhang Fangle et al (2005) Resistivity drop mechanism during heavy oil thermal recovery. Petroleum Exploration and Development 32(2): 116–118

Yang Zhi, Zou Caineng, Fu Jinhua et al (2019) Characteristics and "Sweet Area (Section)" Evaluation of Continuous Tight & Shale Oil and Gas in Ordos Basin, North-central China. Journal of Earth Sciences and Environment 41(04): 459–474

Yang Sheng (1986) A single apparent resistivity expression for loop-offset transient electromagnetics. Geophysics 51(6): 1291–1297

Yan Zhengwen, Tan Handong, Peng Miao et al (2020) Three-dimensional joint inversion of gravity, magnetic and magnetotelluric data based on cross-gradient theory. Chinese Journal of Geophysics (in Chinese) 63(2): 736–752. doi:10.6038/cjg2020M0355

Yuan B, Diquan L, Bayless RC (2017) Wide field Electromagnetic Method for Shale Gas Exploration in Southern China: A case Study. Journal of Environmental & Engineering Geophysics 22(3): 279–289. doi:10.2113/jeeg22.3.279

Yuan Guiqin, Sun Yue, Gao Weidong et al (2013) Development Status of the Shale Gas Geophysical Prospecting Technology. Geology and Explploration 49(5): 945–950

Zhang Chunhe, Liu Xuejun, He Lanfang et al (2013) A study of exploration organic rich shales using Time-Frequency Electromagnetic Method(TFEM). Chinese Journal of Geophysics (in Chinese) 56(9): 3173–3183. doi:10.6038/cjg20130930

Zhang Qiaoxun, Li Diquan, Tian Maojun (2017) Application of wide field electromagnetic method to the hydrocarbon exploration in a basin of South Jiangxi. Oil Geophysical Prospecting 52(5): 1085–1092.

Zhdanov M (2008) Generalized effective-medium theory of induced polarization. Geophysics 73(5): F197–F211

Zhdanov MS, Gribenko AV, Wilson GA, Funk C (2012) 3D joint inversion of geophysical data with Gramian constraints: A case study from the Carrapateena IOCG deposit, South Australia. The Leading Edge 12: 1382–1388

Zhou Cong, Tang Jingtian, Pang Cheng, Hu Shuanggui (2019) A theory and simulation study on the space-time array hybrid source electromagnetic method. Chinese Journal of Geophysics (in Chinese) 62(10): 3827–3842

Zhuo Xianjun et al (2007) Preliminary application of WEM in geophysical exploration. Progress in Geophysics 22(6): 1921–1924

Zonge KL, Wyna JC (1975) recent advance and application in complex resisivity measurement. Geophysics 40(5): 851–864. doi:10.1190/1.1440572

Zou Caineng, Zhang Guosheng, Yang Zhi et al (2013) Geological concepts, characteristics, resource potential and key techniques of unconventional hydrocarbon: On unconventional petroleum geology. Petroleum Exploration and Development 40(4): 385–399

Zou Caineng, Dong Dazhong, Wang Yuman et al (2015) Shale gas in China: Characteristics, challenges and prospects (I). Petroleum Exploration and Development 42(6): 689–701

Zou Caineng, Tao Shizhen, Bai Bin et al (2015) Differences and Relations between Unconventional and Conventional Oil and Gas. China Petroleum Exploration 20(1): 1–16

Zou Caineng, Zhai Guangming, Zhang Guangya et al (2015) Formation, distribution, potential and prediction of global conventional and unconventional hydrocarbon resources. Petroleum Exploration and Development 42(1): 13–25

Zou Caineng, Zhang Guosheng, Yang Zhi et al (2013) Geological concepts, characteristics, resource potential and key techniques of unconventional hydrocarbon: On unconventional petroleum geology. Petroleum Exploration and Development 40(4): 385–399

Zou Caineng, Zhu Rukai, Bai Bin et al (2015) Significance, Geologic Characteristics, Resource Potential and Future Challenges of Tight Oil and Shale Oil. Bulletin of Mineralogy, Petrology and Geochemistry 34(1): 3–17

Table 1. the laboratory measurement

Stratum	Lithology	Rock Number	Density (g/cm3)	Magneti sability (10⁻⁵SI)	Permea bility (mD)	Vp (m/s)	Vs (m/s)	Resistivity (Ohm-m)	Polarizability (%)
Longmaxi Group, Silurian	Shale	52	2.54	2.4	1.232	3580.00	2309.80	111.2	18.1
Wufeng Group, Ordovician	Shale	5	2.52	3.3	0.001	4898.94	2880.18	168.7	21.7
Qiongzhusi Group, Cambrian	Shale	112	2.43	5.4	0.933	4178.00	2623.62	147.0	42.5
Dengying Group, Sinian	Dolomite	23	2.81	1.9	3.606	4278.00	2877.97	2507.8	12.5

Table 3. the electric model and the model space for the PM area

Layer number	Thickness and model space (m)	Resistivity and model space ($\Omega \cdot m$)	Polarizability and model space
1	40(39.6,40.4)	80(50,100)	0.040(0.010,0.150)
2	110(109.9,110.1)	20(5,80)	0.120(0.010,0.200)
3	175(173.3,176.8)	10(1,30)	0.060(0.010,0.250)
4	250(2247.5,252.5)	50(10,70)	0.150(0.050,0.500)
5	140(138.6,141.4)	5(2,15)	0.050(0.010,0.350)
6	50(49.5,50.5)	10(5,15)	0.150(0.010,0.350)
7	50(49.5,50.5)	25(20,80)	0.250(0.010,0.450)
8	60(59.4,60.6)	70(1.5,200)	0.400(0.050,0.700)
9	90(89.1,90.9)	15(5,20)	0.100(0.010,0.400)
10	700(693.0,707.0)	20(2.5,100)	0.010(0.005,0.100)
11	450(445.5,454.5)	5(1.5,20)	0.075(0.010,0.150)
12	650(643.5,656.5)	2000(1950,2050)	0.005(0.000,0.001)
13	100(99.0,101.0)	50(10.80)	0.010(0.001,0.100)
14	400(396.0,404.0)	200(150,300)	0.100(0.010,0.200)
15	180(178.2,181.8)	500(100,2000)	0.120(0.010,0.200)
16	1000(990.0,1010.0)	1000(300,2000)	0.150(0.010,0.200)

Table 5. Geo-Resistivity model based on JIAOYE #1 Logging curve

Stratigraphy	Lithology	Burial depth(m)	Thickness(m)	Resistivity （Ω·m)
P$_2$ch-C2hl	Limestone	0--1430	1430	>2000
S$_2$h-S$_1$l	Mudstone	1430--2290	860	30-40
S$_1$l	Sandstone	2290--2330	40	244
S$_1$l -O$_3$w	Gas-bearing shale	2330--2410	80	42
O$_3$-O$_1$	Limestone	2410—		>1000

Table 6. Production information record of shale gas fracturing in test horizontal wells

Well section number	Fracturing date	Fracturing Start Time	Fracturing Termination Time	Fluid/Proppant Volume (m³)
XX-6	February 29, 2016	18:07:23	20:35:03	1849.9/40.4
XX-7	March 1, 2016	08:41:33	11:37:00	1955.6/49.6
XX-8	March 1, 2016	17:07:50	19:53:00	1847.7/48.1